Article

Cell

# Systematic Immunotherapy Target Discovery Using Genome-Scale *In Vivo* CRISPR Screens in CD8 T Cells

## Graphical Abstract

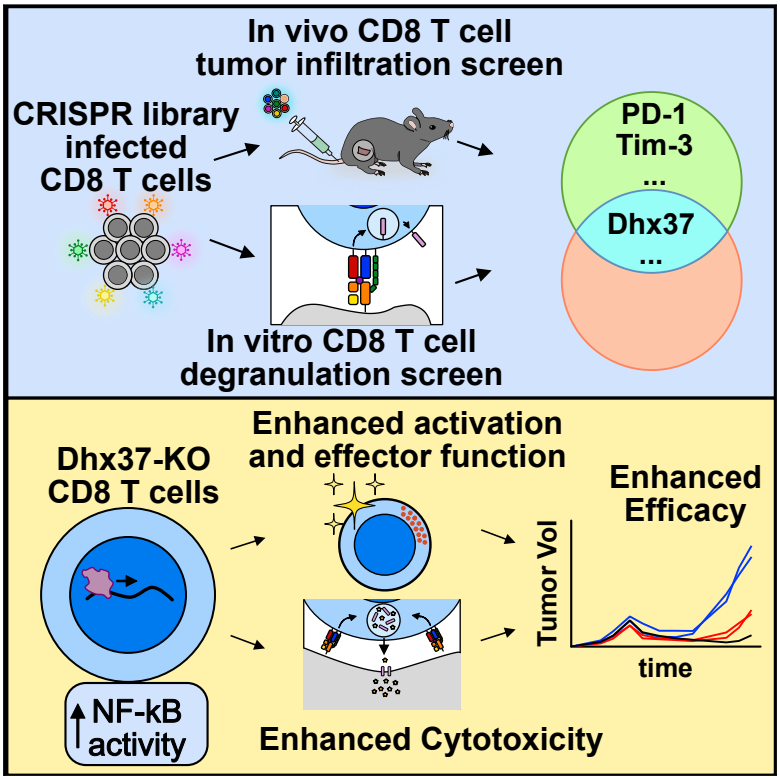


## Highlights

- *In vivo* and *in vitro* genome-scale CD8 T cell CRISPR screen in immunotherapy contexts
- *Dhx37* knockout in CD8 T cells enhances adoptive transfer efficacy
- Dhx37 modulates CD8 T cell activation, cytokine production, and cytotoxicity
- DHX37 interacts with PDCD11 and influences NF-κB activity

## Authors

Matthew B. Dong, Guangchuan Wang, Ryan D. Chow, ..., Donald R. Lannin, Roy S. Herbst, Sidi Chen

## Correspondence

sidi.chen@yale.edu

## In Brief

Genome-wide CRISPR screening in CD8 T cells in the context of immunotherapy identifies genes that modulate T cell effector functions, including *Dhx37*, an RNA helicase that affects NF-κB signaling, T cell activation, and cytotoxicity.

Dong et al., 2019, Cell *178*, 1189–1204
August 22, 2019 
https://doi.org/10.1016/j.cell.2019.07.044

CellPress

Cell

# Systematic Immunotherapy Target Discovery Using Genome-Scale *In Vivo* CRISPR Screens in CD8 T Cells

Matthew B. Dong,[1,2,3,4,5,6,19] Guangchuan Wang,[1,2,3,19] Ryan D. Chow,[1,2,3,4,19] Lupeng Ye,[1,2,3,19] Lvyun Zhu,[1,2,3] Xiaoyun Dai,[1,2,3] Jonathan J. Park,[1,2,3,4] Hyunu R. Kim,[1,2,3] Youssef Errami,[1,2,3] Christopher D. Guzman,[1,2,3,5,6,7] Xiaoyu Zhou,[1,2,3] Krista Y. Chen,[1,2,3,8] Paul A. Renauer,[1,2,3,7] Yaying Du,[1,2,3] Johanna Shen,[1,2,3,8] Stanley Z. Lam,[1,2,3,8] Jingjia J. Zhou,[1,2,3,8] Donald R. Lannin,[9,10,13,14] Roy S. Herbst,[11,12,13,14] and Sidi Chen[1,2,3,4,5,7,14,15,16,17,18,20,*]

[1]Department of Genetics, Yale University School of Medicine, 333 Cedar Street, New Haven, CT 06520, USA
[2]System Biology Institute, Integrated Science & Technology Center, Yale University, 850 W Campus Drive, West Haven, CT 06516, USA
[3]Center for Cancer Systems Biology, Integrated Science & Technology Center, Yale University, 850 W Campus Drive, West Haven, CT 06516, USA
[4]Yale MD-PhD Program, Yale University School of Medicine, New Haven, CT 06510, USA
[5]Immunobiology Program, Yale University School of Medicine, New Haven, CT 06510, USA
[6]Department of Immunobiology, Yale University School of Medicine, New Haven, CT 06510, USA
[7]Combined Program in the Biological and Biomedical Sciences, Yale University School of Medicine, New Haven, CT 06510, USA
[8]The College, Yale University, New Haven, CT 06520, USA
[9]Department of Surgery, Yale University School of Medicine, New Haven, CT 06510, USA
[10]Breast Cancer Program, Yale University School of Medicine, New Haven, CT06510, USA
[11]Department of Medicine, Yale University School of Medicine, New Haven, CT 06510, USA
[12]Department of Pharmacology, Yale University School of Medicine, New Haven, CT 06510, USA
[13]Smilow Cancer Hospital, 35 Park Street, New Haven, CT 06510
[14]Yale Comprehensive Cancer Center, Yale University School of Medicine, New Haven, CT 06510, USA
[15]Department of Neurosurgery, Yale University School of Medicine, New Haven, CT 06510, USA
[16]Yale Stem Cell Center, Yale University School of Medicine, New Haven, CT 06510, USA
[17]Yale Liver Center, Yale University School of Medicine, New Haven, CT 06510, USA
[18]Yale Center for Biomedical Data Science, Yale University School of Medicine, New Haven, CT 06510, USA
[19]These authors contributed equally
[20]Lead Contact
*Correspondence: sidi.chen@yale.edu
https://doi.org/10.1016/j.cell.2019.07.044

## SUMMARY

CD8 T cells play essential roles in anti-tumor immune responses. Here, we performed genome-scale CRISPR screens in CD8 T cells directly under cancer immunotherapy settings and identified regulators of tumor infiltration and degranulation. The *in vivo* screen robustly re-identified canonical immunotherapy targets such as PD-1 and Tim-3, along with genes that have not been characterized in T cells. The infiltration and degranulation screens converged on an RNA helicase *Dhx37*. *Dhx37* knockout enhanced the efficacy of antigen-specific CD8 T cells against triple-negative breast cancer *in vivo*. Immunological characterization in mouse and human CD8 T cells revealed that DHX37 suppresses effector functions, cytokine production, and T cell activation. Transcriptomic profiling and biochemical interrogation revealed a role for DHX37 in modulating NF-κB. These data demonstrate high-throughput *in vivo* genetic screens for immunotherapy target discovery and establishes DHX37 as a functional regulator of CD8 T cells.

## INTRODUCTION

T cells play a central role in maintaining the cellular integrity of the body against intracellular pathogens and tumors (Kaech et al., 2002; Tscharke et al., 2015; Zhang and Bevan, 2011). Activation of antigen-specific CD8 T cells is mediated by T cell receptor (TCR) recognition of cognate antigen on surface major histocompatibility complex (MHC) class I (MHC-I) (Blum et al., 2013; Cox et al., 2011; Tscharke et al., 2015), resulting in T cell proliferation, cytokine production, and killing of target cells (Wong and Pamer, 2003). Defects in T cells can lead to recurrent infections (Dumontet et al., 2015; Hersperger et al., 2011; Kurktschiev et al., 2014; Zhang et al., 2009) or cancer (Chia et al., 2009; Clementi et al., 2005; Mortaz et al., 2016), while dysregulated activation of $CD8^+$ T cells can result in immunopathology and autoimmunity (Gravano and Hoyer, 2013; Holzelova et al., 2004; Valori et al., 2017; Walter and Santamaria, 2005). CD8 T cells have become the central focus of new cancer therapeutics (Blankenstein et al., 2012; Chen and Mellman, 2013; Fridman et al., 2012;

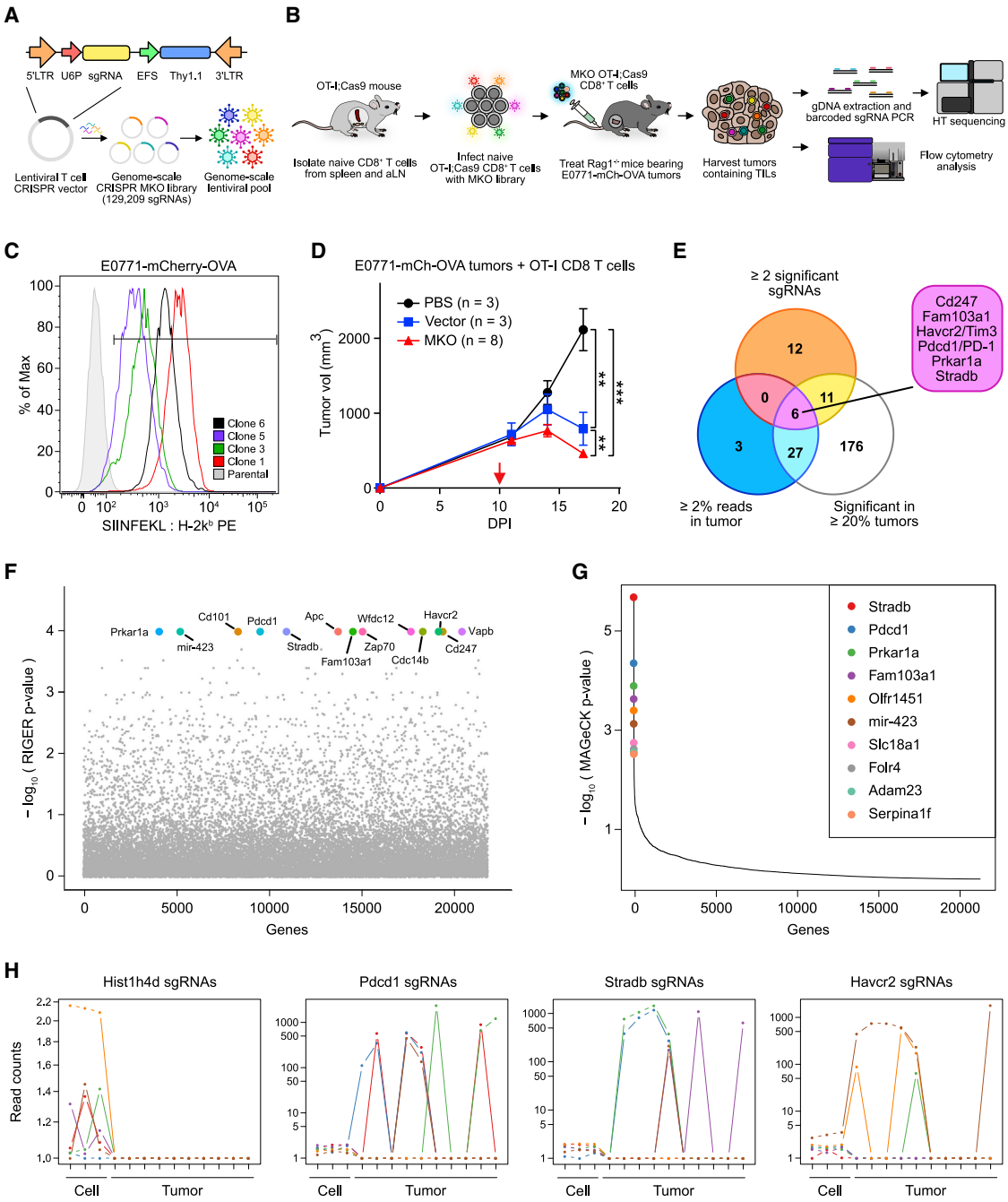


**Figure 1. Genome-Scale *In Vivo* CD8 T Cell Screen Identified Genes Regulating Tumor Infiltration**

(A) Schematics of the design of a T cell CRISPR vector, MKO library cloning, and lentiviral library production.

(B) Schematics of experiment design.

(C) Measurement of antigen presentation in E0771-mCh-OVA clonal cell lines with a SIINFEKL:H-2k$^{b}$ antibody.

(D) Growth curve of intramammary fat pad tumors from transplanted E0771-mCh-OVA cells in *Rag1*$^{-/-}$ mice following different treatments. PBS control (n = 3), adoptive transfer of OT-I;Cas9 CD8 T cells infected with vector (n = 3) or MKO (n = 8). Red arrow indicates the time of adoptive transfer. Data are shown as mean ± SEM. Note that some error bars are not visible because the values are small. *p < 0.05, **p < 0.01, ***p < 0.001 by two-way ANOVA.

(E) Venn diagram of the three enrichment criteria to identify the top gene hits (≥2% read abundance in one sample [n = 36], significant in ≥20% of samples [n = 220], and ≥2 independent enriched sgRNAs [n = 26]).

(F) Meta-analysis of infiltration screen using RIGER with the second-best sgRNA method.

*(legend continued on next page)*

Spranger et al., 2013). Approved immune checkpoint inhibitors enhance anti-tumor response of CD8 T cells by neutralizing CTLA-4 or PD-1/PD-L1 (Brahmer et al., 2010; Kvistborg et al., 2014; Pardoll, 2012; Ribas, 2012; Swart et al., 2016; Tumeh et al., 2014). These drugs have been effective in multiple oncology indications (Mellman et al., 2011; Sharon et al., 2014), either as monotherapies or in combination with other therapies (Larkin et al., 2015; Postow et al., 2015). Newer checkpoint inhibitors are now under active investigation, such as TIM-3, LAG3, 4-1BB, CD28, ICOS, OX-40, and VISTA (Johnson and June, 2017; Mahoney et al., 2015). Meanwhile, cellular therapeutics utilizing CD8 T cells with chimeric antigen receptors (CARs) (Fesnak et al., 2016; Srivastava and Riddell, 2015) have demonstrated clinical success against hematopoietic malignancies (Esensten et al., 2016; Jackson et al., 2016; Johnson and June, 2017) and have been recently approved. Discovery of previously unknown genes that modulate T cell function is of urgent need to open different avenues for immunotherapies (Mellman et al., 2011), as a large fraction of patients still do not respond to, or have undesired side effects to currently approved therapies (Kelderman et al., 2014; Restifo et al., 2016). Systematic approaches to identify new regulators of T cell functions *in vivo* can provide potentially orthogonal or complementary opportunities (Ghoneim et al., 2016).

Studies using RNAi or shRNA (short hairpin RNA) libraries have been used to identify CD8 T cell regulators (Chen et al., 2014; Zhou et al., 2014). RNAi operate by degrading mRNA or suppressing their translation but have substantial off-target effects (Nijman, 2015). CRISPR technologies have dramatically enhanced our ability in genome editing (Cong et al., 2013; Hsu et al., 2014; Jinek et al., 2012; Komor et al., 2017; Mali et al., 2013; Wright et al., 2016). High-throughput CRISPR screens have been developed for discovery of novel genes (Shalem et al., 2014; Wang et al., 2014; Shalem et al., 2015). Application of CRISPR technologies has enabled the manipulation of the T cell genome (Beil-Wagner et al., 2016; Singer et al., 2016; Su et al., 2016). Genetic screens have been performed *in vitro* for discovery of regulators for T cell proliferation and differentiation (Henriksson et al., 2019; Shifrut et al., 2018). Given the complexity of physiological cues, it is critical to perform *in vivo* screens to better identify clinically relevant targets. High-throughput *in vivo* CRISPR screens in primary CD8 T cells would enable rapid identification of negative regulators of T cell anti-tumor function, thereby providing potential targets for immunotherapy.

In this study, we performed *in vivo* genome-scale CRISPR screens in CD8 T cells for tumor infiltration in mouse models of triple-negative breast cancer (TNBC). Our screen re-discovered prime immunotherapy targets such as PD-1 and Tim-3, as well as previously undocumented targets. We also performed an orthogonal screen to identify factors that modulate CD8 T cell degranulation ability. The screens converged on a small number of hits that included *Dhx37*, a previously uncharacterized target in T cells. We subsequently interrogated the function of *Dhx37*/*DHX37* in both mouse and human CD8 T cells. Our data revealed that Dhx37 suppresses CD8 T cell activity in response to antigenic stimulation. Biochemical experiments along with transcriptome profiling revealed that DHX37 interacts with both nuclear factor κB (NF-κB) p65 and PDCD11 and modulates NF-κB pathway activity in CD8 T cells.

## RESULTS

### Development of Genetic Screens of *In Vivo* Tumor Infiltration and Cytotoxic Function in Primary CD8 T Cells

We designed and generated a lentiviral CRISPR vector that contains an sgRNA expression cassette and Thy1.1 (STAR Methods) (Figure 1A). Next, we cloned into this vector a mouse genome-scale single guide RNA (sgRNA) library (MKO) containing 128,209 gene-specific sgRNAs and 1,000 non-targeting controls (NTCs) (Table S1). We generated lentivirus from this library (Figures 1A and 1B) (STAR Methods), which enabled T cell CRISPR screens.

To set up a model system for T cell immunotherapy screens, we utilized E0771 cells, a murine TNBC line, as a transplant tumor model (Figure 1B). To enable T cell recognition of cognate antigen in cancer cells, we generated clonal E0771 cell lines that constitutively express chicken ovalbumin (OVA) (STAR Methods) (Figure 1C). Using an antibody that recognizes the SIINFEKL: H-2K$^b$ complex (Porgador et al., 1997), we confirmed that the SIINFEKL epitope of OVA was presented on surface H-2K$^b$ (Figure 1C). Clone 3 of E0771-mCherry-OVA (E0771-mCh-OVA) cell lines was chosen for further studies because it presented a low-level, single-peak SIINFEKL: H-2K$^b$ (Figure 1C). We then isolated naive CD8$^+$ T cells from OT-I;Cas9 mice, cultured for 3 days, and then adoptively transferred these cells into *Rag1*-deficient mice (Figure S1A). Prior to adoptive transfer, these cells were analyzed by flow cytometry and found to have upregulated the T cell activation markers, CD44 and CD69 (Figures S1B and S1C). 7 days post-transfer, spleens were isolated and CD8$^+$ T cells were purified and co-cultured with either E0771 or E0771-mCh-OVA cells in the presence of CD107a antibody, a granule-specific marker that is transiently deposited on the surface of T cells in response to antigenic stimulation (Betts et al., 2003), to quantitatively measure the degree of T cell degranulation (degranulation assay) (STAR Methods) (Figure S1D). We found that the transferred OT-I;Cas9 CD8 T cells degranulated in the presence of OVA, demonstrating that the transferred T cells retained antigenic specificity (Figure S1E). To determine whether the observed anti-tumor responses were OVA specific, we performed an *in vivo* experiment using E0771 cells or E0771-mCh-OVA cells transplanted into the mammary fat pad of *Rag1*$^{-/-}$ female mice. After 10 days, these mice were treated with either PBS or OT-I;Cas9 CD8 T cells (Figure S1F). We found that tumor regression occurred only in mice bearing E0771-mCh-OVA tumors treated with OT-I;Cas9 CD8$^+$ T cells but not

(G) Meta-analysis of infiltration screen using MAGeCK analysis of survival screen.
(H) Single gene-level analysis of individual for their sgRNA distributions across each sample, showing representative genes depleted (*His1h4d*) or enriched (*Pdcd1*, *Stradb*, and *Havcr2*) in tumors as compared to cells.
See also Figures S1, S3, and S3 and Table S1.

in the groups treated with either PBS or in mice carrying E0771 tumors (Figure S1G). Together, these data confirmed the antigenic specificity of this model system, providing a normalized baseline for *in vivo* genetic screens in primary CD8 T cells.

We then performed the *in vivo* T cell tumor infiltration screen (Figure 1B), using a mammary fat pad orthotopic tumor model (Figure 1D), as well as a subcutaneous model in parallel (Figures S2A and S2B) (STAR Methods). We transduced $CD8^+$ T cells from OT-I;Cas9 mice with the MKO sgRNA library and adoptively transferred them into E0771-OVA tumor-bearing mice bearing tumors (STAR Methods). In both orthotopic and subcutaneous models, we observed that T cell injections (either vector or MKO transduced) mitigated tumor growth and that the MKO transduced population had a stronger therapeutic effect compared to vector control (Figure 1D). Histological and pathological analysis revealed the presence of tumor-infiltrating lymphocytes (TILs) from mice receiving adoptive transfer but not in PBS-treated mice (Figure S2B). Flow cytometric analysis of single-cell suspensions of spleens, lymph nodes, and tumors also detected adoptively transferred $CD8^+$ T cells (Figure S2C). Tumors from a cohort of mice were subjected to high-throughput sgRNA library sequencing (STAR Methods), which revealed the sgRNA representations of MKO transduced OT-I;Cas9 CD8 T cells before injection and in all tumor samples (Table S1; Figures S2D and S2E). While the library representation of pre-injected T cells follows a log-normal distribution for both gene-targeting sgRNAs and NTCs, the sgRNA representation in organs is characterized by the dominance of a small fraction of sgRNAs (Figure S2D). At the individual mouse level, we found that the sgRNA representation between different mice are correlated with each other (Figure S2E).

## Convergent T Cell Screens Identified Known and Undocumented Immunotherapy Targets

Using stringent criteria (false discovery rate [FDR] <0.5%), we identified significantly enriched sgRNAs in each tumor (STAR Methods). A composite of multiple ranking approaches, including sgRNA abundance, multiple independent sgRNAs and multiple mouse replicates (STAR Methods), revealed rank lists of top scoring sgRNAs and genes (Figure 1E; Figures S3A ad S3B). The infiltration screen revealed high-rank genes representing three classes of genes: immune regulators, growth controlling genes, and largely uncharacterized genes (Figures 1E–1G; Figures S3A and S3B). A total of 6 genes were significantly enriched with all three criteria fulfilled (*Cd247*, *Fam103a1*, *Hacvr2/Tim-3*, *Pdcd1/PD-1*, *Prkar1a*, and *Stradb*) (Figure 1E). To further assess the robustness of screen performance, we first applied RIGER (STAR Methods), an analysis method considering the performance of multiple sgRNAs for the same gene. RIGER analysis with the $2^{nd}$-best sgRNA method revealed 13 genes at top-level statistical significance ($p \leq 1e\text{-}4$) (Figure 1F), while the weighted-sum method scored 7 genes at top significance (Figure S3C), where 6 of them were shared with the $2^{nd}$-best sgRNA method. In fact, these six genes (*Cd247*, *Fam103a1*, *Hacvr2*, *Pdcd1*, *Prkar1a*, and *Stradb*) are exactly identical to the 3-way shared hits identified by our custom FDR method. We also performed a parallel analysis with MAGeCK, a model-based algorithm for genome-scale CRISPR screens (Li et al., 2014), which again revealed *Stradb*, *Pdcd1*, *Prkar1a*, and *Fam103a1* on top of the list (Figure 1G; Figure S3D). Examination of individual genes revealed strongly depleted sgRNAs targeting essential genes (e.g., *Hist1h4d*) and enriched sgRNAs targeting known or potentially new T cell phenotype modulators (Figure 1H). PD-1 and Tim-3 are well-known immunotherapy targets, thereby benchmarking the success and technical rigor of the screen. Collectively, these analyses demonstrate the rigor of *in vivo* CRISPR screen for CD8 T cell tumor infiltration and revealed targets for cancer immunotherapy.

We set out to independently identify genes that could modulate the ability of CD8 T cells to kill cancer cells. We performed a screen using degranulation assay (Figure 2A). We pulsed E0771 cells with varying concentrations of SIINFEKL peptide and found that they presented SIINFEKL peptide on surface MHC-I in a dose-dependent manner (Figure 2B). We isolated naive OT-I;Cas9 CD8 T cells and transduced them with MKO library, stimulated them for 6 days, rested them for 12 h, and then co-cultured them with SIINFEKL-pulsed E0771 cells at 1:1 of T cell: cancer cell (Effector: Target, or E: T) ratio in the presence of CD107a antibody (STAR Methods) (Betts et al., 2003). With three biological replicates, we sorted the top 5% $CD107a^+$ cells (Figure 2C) and then subjected them to screen readout and data analysis (STAR Methods). Using the FDR <0.5% significance cutoff, we identified significantly enriched sgRNAs and their corresponding genes (Figure 2D), which represented potential negative regulators of T cell degranulation. Three genes emerged as common hits between the degranulation screen and the tumor infiltration screen (*Dhx37*, *Lyn*, and *Odc1*) (Figure 2E).

## Immunotherapeutic Potential of *Dhx37* Gene-Edited CD8 T Cells

To examine the function of these genes in a model of immunotherapy, we cloned sgRNAs targeting *Dhx37* and *Odc1* that scored in both screens, along with *Pdcd1* (which only scored in the infiltration screen) into the T cell lentiviral CRISPR vector. We did not pursue *Lyn* because it is not normally expressed in T cells (Tsantikos et al., 2009; Yamanashi et al., 1989). We then prepared lentivirus, transduced T cells, and adoptively transferred them into mice bearing E0771-mCh-OVA tumors (STAR Methods). Despite initially growing for 3 days post-adoptive transfer, the tumors treated by adoptive T cells regressed over the following 2.5 weeks (Figures 2F and 2G). All OT-I;Cas9 CD8 T cell-treatment groups demonstrated strong anti-tumor effects beginning 7 days after adoptive transfer (Figure 2G). Notably, sgDhx37 infected OT-I;Cas9 CD8 T cells significantly suppressed relapse when compared to mice treated with vector-infected T cells (Figure 2G). We observed that (5/5, 100%) of the mice in the sgDhx37 group had smaller tumors as compared to the vector group, compared to 2/5 in sgPdcd1 and 3/5 in sgOdc1 groups (Figure 2H). These data suggest that CRISPR targeting of *Dhx37* enhanced the anti-tumor effects of OT-I;Cas9 CD8 T cells against E0771-mCh-OVA tumors.

## Analysis of Gene Expression Signatures in *Dhx37* Tumor-Infiltrating Lymphocytes by Single-Cell RNA-Seq

Dhx37 is a highly conserved DEAH box RNA helicase that has been reported to be involved with biogenesis of the small

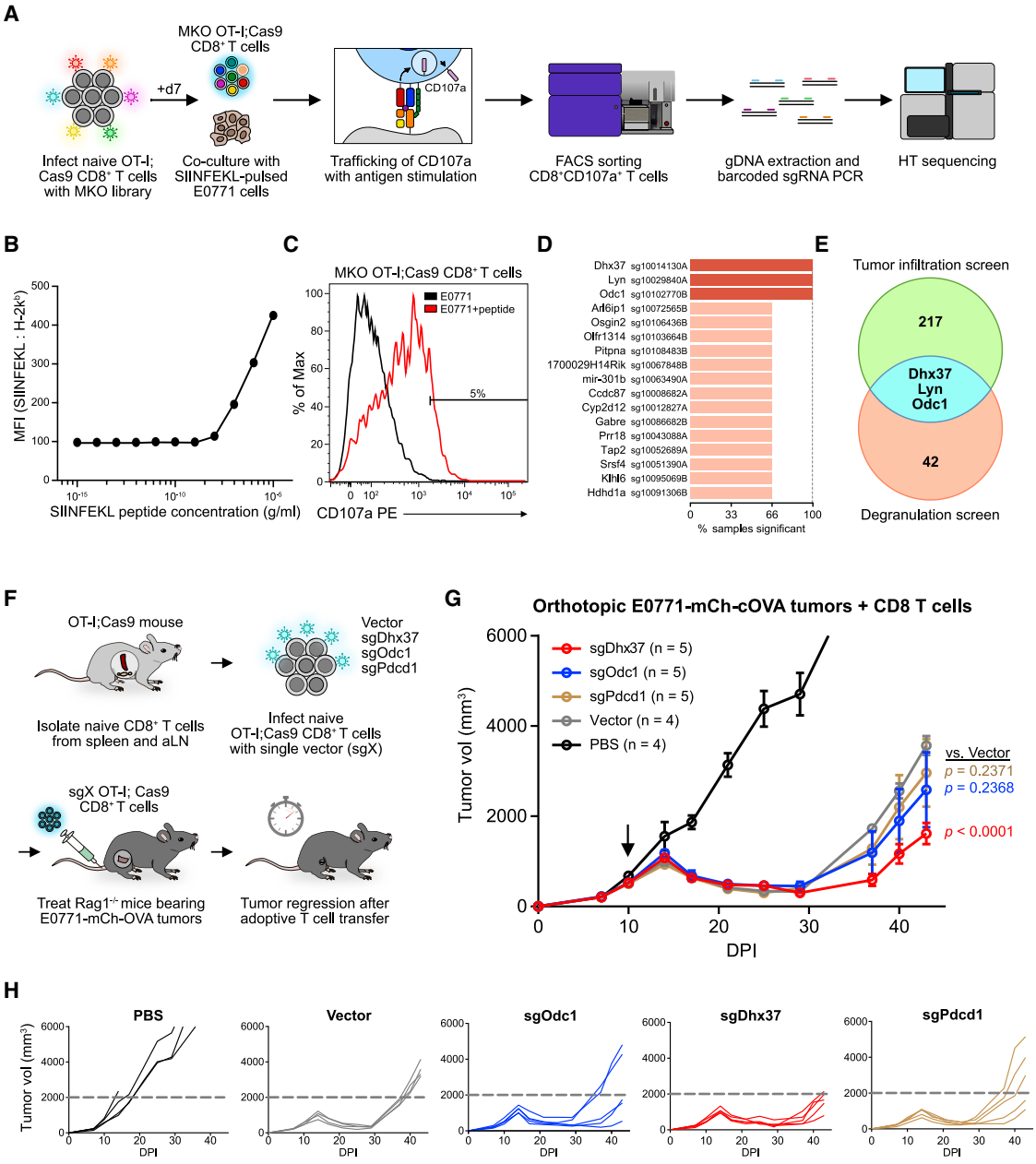


**Figure 2. High-Throughput CRISPR Screen of CD8 T Cell Degranulation Identified *Dhx37* and *Odc1* as Top Hits Convergent with Infiltration**

(A) Schematics of experiment.

(B) Titration of SIINFEKL peptide on MHC-I in E0771 cells.

(C) Representative histogram of CD107a$^{+}$ T cells analyzed from the co-culture of OT-I;Cas9 CD8 T cells and E0771 cancer cells.

(D) Waterfall plot of the top-ranked sgRNAs across all sorted cell samples.

(E) Venn diagram comparing the hits from the degranulation screen and from the tumor infiltration screen.

(F) Schematics of efficacy testing experiments with adoptive transfer of single-gene knockout CD8 T cells

(G) Growth curves of mammary fat pad E0771-mCh-OVA tumors in *Rag1*$^{-/-}$ mice following different treatments: PBS control, adoptive transfer of OT-I;Cas9 CD8 T cells infected with lentiviral vector, lenti-sgDhx37, lenti-sgOdc1, and lenti-sgPdcd1. Note: arrow indicates the time of adoptive transfer of MKO or vector transduced OT-I; Cas9 CD8 T cells. Data are shown as mean ± SEM. Statistical comparisons were made with two-way ANOVA for each group against vector, with p values indicated.

(H) Spider plots of (G) separated by treatment group for visibility.

See also Figures S4 and S5.

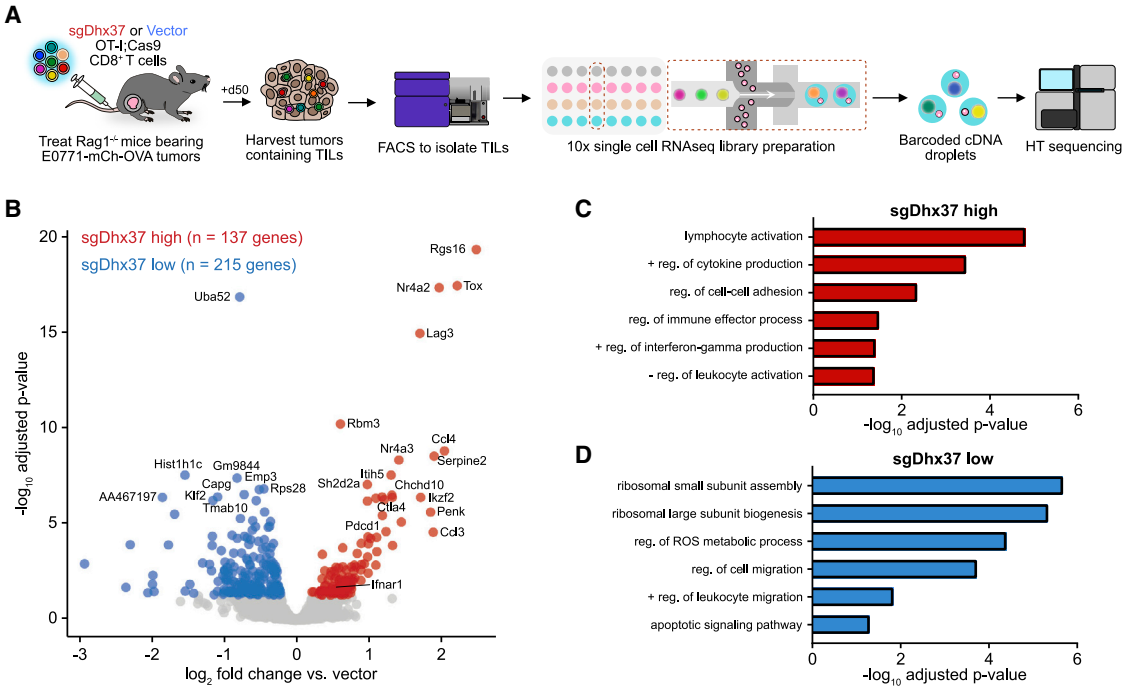


**Figure 3. Single-Cell Transcriptomics of *Dhx37* Knockout CD8 Tumor-Infiltrating Lymphocytes**

(A) Schematics of experiment.

(B) Volcano plot of differentially expressed genes in tumor-infiltrating CD8 cells treated with sgDhx37 compared to vector control.

(C) Gene Ontology (GO) analysis of significantly upregulated genes in sgDhx37-treated tumor-infiltrating CD8 cells.

(D) GO analysis of significantly downregulated genes in sgDhx37-treated tumor-infiltrating CD8 cells.

Note: for (C) and (D), significantly enriched (Bonferroni adjusted $p < 0.05$) GO categories were shown. See also Table S2.

ribosomal subunit through its release of U3 small nucleolar RNA (snoRNA) (Roychowdhury et al., 2019). Its homologs have also been found to regulate escape behavior via glycine receptor expression in zebrafish (Hirata et al., 2013) and cause microcephaly in rare gene variants (Karaca et al., 2015). However, this gene has not been previously associated with T cell function. The putative ATP-dependent RNA helicase domain and conservation implies that it might affect gene expression (Abdelhaleem, 2005). Because the heterogeneous tumor microenvironment might influence the functional state of individual TILs, we performed single-cell RNA sequencing (scRNA-seq) to investigate the transcriptomes of adoptively transferred sgDhx37-transduced OT-I;Cas9 CD8 TILs (sgDhx37 TILs) (Figure 3A) (STAR Methods).

After processing, stringent filtering and normalizing the raw scRNA-seq data (STAR Methods), the TIL scRNA-seq dataset was composed of 552 cells (sgDhx37, n = 191 cells; vector, n = 361 cells), collectively measuring 8,244 expressed genes in TILs (Table S2). We performed differential expression analysis between sgDhx37- and vector-treated TILs, identifying sets of significantly upregulated and downregulated genes (Table S2). 215 genes were significantly downregulated in sgDhx37 TILs, while 137 genes were significantly upregulated (Benjamini-Hochberg adjusted $p < 0.05$), with the mostly highly upregulated genes being *Rgs16*, *Tox*, and *Nr4a2* (Figure 3B). *Tox* has been recently implicated as a critical regulator of CD8 T cell and TILs (Alfei et al., 2019; Khan et al., 2019; Scott et al., 2019). NR4A family members were found to regulate CAR-T potency against solid tumors (Chen et al., 2019). Other significantly upregulated genes included known immune-related genes such as *Eomes*, *Nr4a3*, *Ccl4*, *Ifnar1*, and *Ikzf2* (Figure 3B; Table S2). The sgDhx37-upregulated genes also include genes involved in negative regulation of leukocyte activation such as *Ctla4*, *Lag3*, and *Pdcd1*, albeit to a lesser extent, which mirrors the positive correlation of T cell cytotoxic scores with these markers in TILs from human melanoma patients (Tirosh et al., 2016). As a gene set, gene ontology (GO) analysis revealed multiple immune-related pathways that were significantly upregulated in sgDhx37 TILs (adjusted $p < 0.05$), including lymphocyte activation, positive regulation of cytokine production, regulation of cell-cell adhesion, regulation of immune effector process, and positive regulation of interferon-gamma (IFN-γ) production (Figure 3C). Downregulated genes in sgDhx37 TILs are enriched in ribosomal small subunit assembly and ribosomal large subunit biogenesis (Figure 3D), consistent with its known role in rRNA modification and processing. Taken together, the scRNA-seq data revealed significant changes in the transcriptomes of sgDhx37 TILs in the heterogeneous tumor microenvironment at the single-cell level.

## Validation and Immunologic Characterization of *Dhx37* as a Regulator of Primary CD8 T Cells

We generated an adeno-associated virus (AAV) vector (AAV-sgRNA-Thy1.1) capable of producing bona fide gene editing in

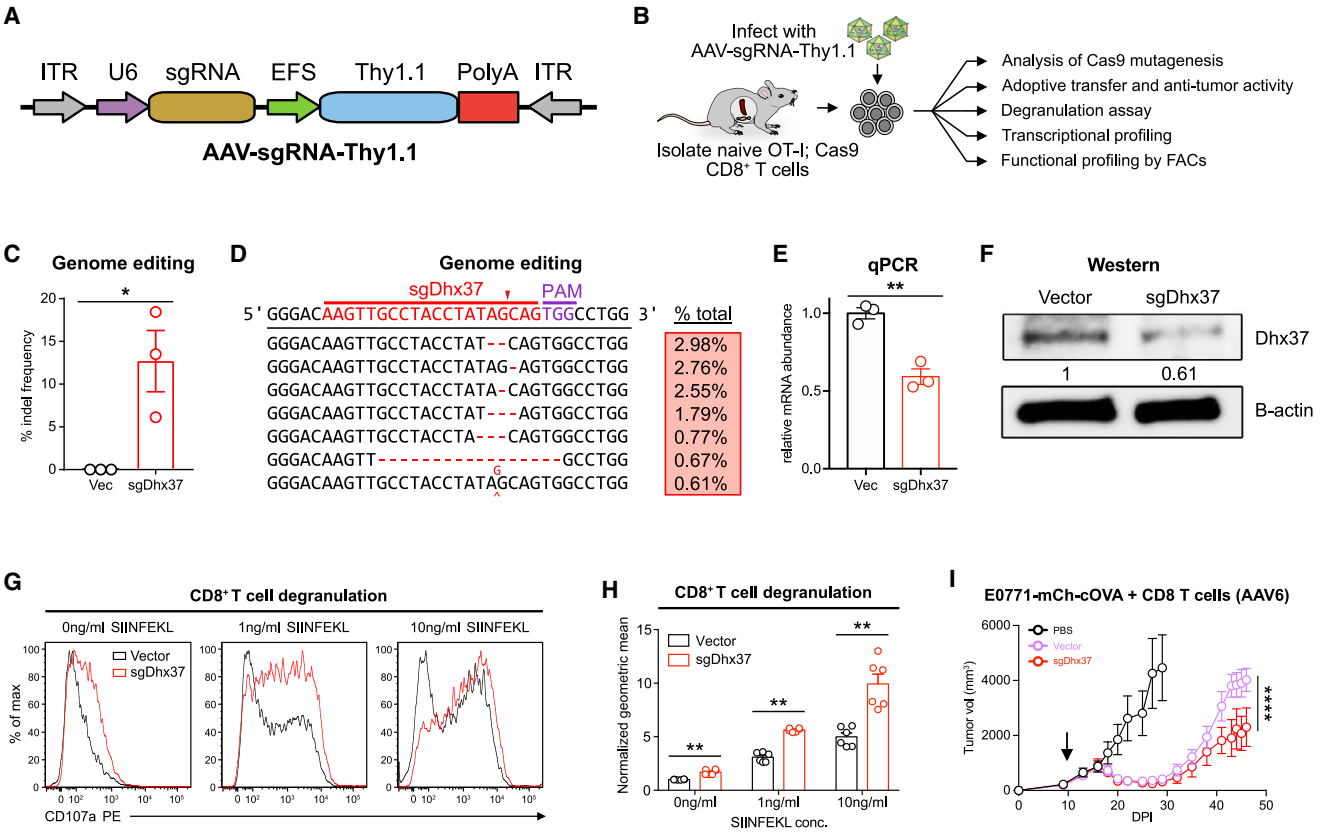


**Figure 4. AAV-Mediated Gene Editing in Primary Murine CD8 T Cells and Effect of *Dhx37* Perturbation**

(A) Schematics of the AAV-CRISPR T cell knockout vector.

(B) Schematics of experiment.

(C) *Dhx37* gene editing in mouse CD8 T cells with AAV-CRISPR measured by T7E1 assay.

(D) Representative Illumina targeted amplicon sequencing of the sgRNA target site 5 days after infection with AAV-sgDhx37. Top most frequent variants were shown, with the associated variant frequencies in the box to the right. PAM and sgRNA spacers were indicated above. Red arrows indicate predicted cleavage sites. Red dashed lines indicate deletions.

(E) qPCR of *Dhx37* mRNA level in murine CD8 T cells with AAV-sgDhx37 transduction.

(F) Western blot of Dhx37 protein level in murine CD8 T cells with AAV-sgDhx37 transduction.

(G) Representative flow histograms of CD107a degranulation assay for *Dhx37* knockout CD8 T cells.

(H) Quantification of data from (G) with independent experimental replicates.

(I) Anti-tumor activity of adoptive transfer of AAV-CRISPR mediated *Dhx37* knockout CD8 T cells. Growth curves of mammary fat pad E0771-mCh-OVA tumors in *Rag1*$^{-/-}$ mice following different treatments.

Note: in all bar plots, data are shown as mean ± SEM. *$p < 0.05$, **$p < 0.01$, ***$p < 0.001$, by unpaired two-sided t test. In tumor growth curves, arrow indicates the time of adoptive transfer. ****$p < 0.0001$ by two-way ANOVA.

See also Figures S4 and S5 and Table S3.

primary murine CD8 T cells (Figure 4A) (STAR Methods). By isolating OT-I;Cas9 CD8 T cells and infecting them with respective AAV vectors, we performed molecular, functional, and immunological analysis of *Dhx37* loss, in addition to anti-tumor efficacy testing (Figure 4B). Amplicon sequencing showed that AAV-sgDhx37 potently mutagenized the targeted loci 5 days post-infection (Figures 4C and 4D; Table S3). This observation is corroborated with a reduction of *Dhx37* mRNA and Dhx37 protein levels in T cells (Figures 4E and 4F). The partial knockdown is likely due to incomplete gene editing efficiency, mRNA and Dhx37 protein stability at this time point, and the fact that not all indels lead to effective loss of protein, which together might under-estimate the effect of *Dhx37* mutagenesis by CRISPR. Despite the incomplete knockout, we observed that compared to vector control, AAV-sgDhx37-treated OT-I;Cas9 CD8 T cells had significantly increased degranulation (surface CD107a) when co-cultured with cognate SIINFEKL-pulsed E0771 cells, at baseline (0 ng/mL), physiological (1 ng/mL), and saturation (10 ng/mL) conditions of anti-CD3 stimulation (Figures 4G and 4H). Moreover, we found no differences in cell growth between sgDhx37 and control T cells in culture (Figure S4A), ruling out the possibility that the degranulation result was simply due to a growth advantage.

Using the same E0771-mCh-OVA tumor model, we again validated that *Dhx37* perturbation by AAV-sgDhx37 showed enhanced efficacy of adoptive T cell therapy (Figure 4I). During

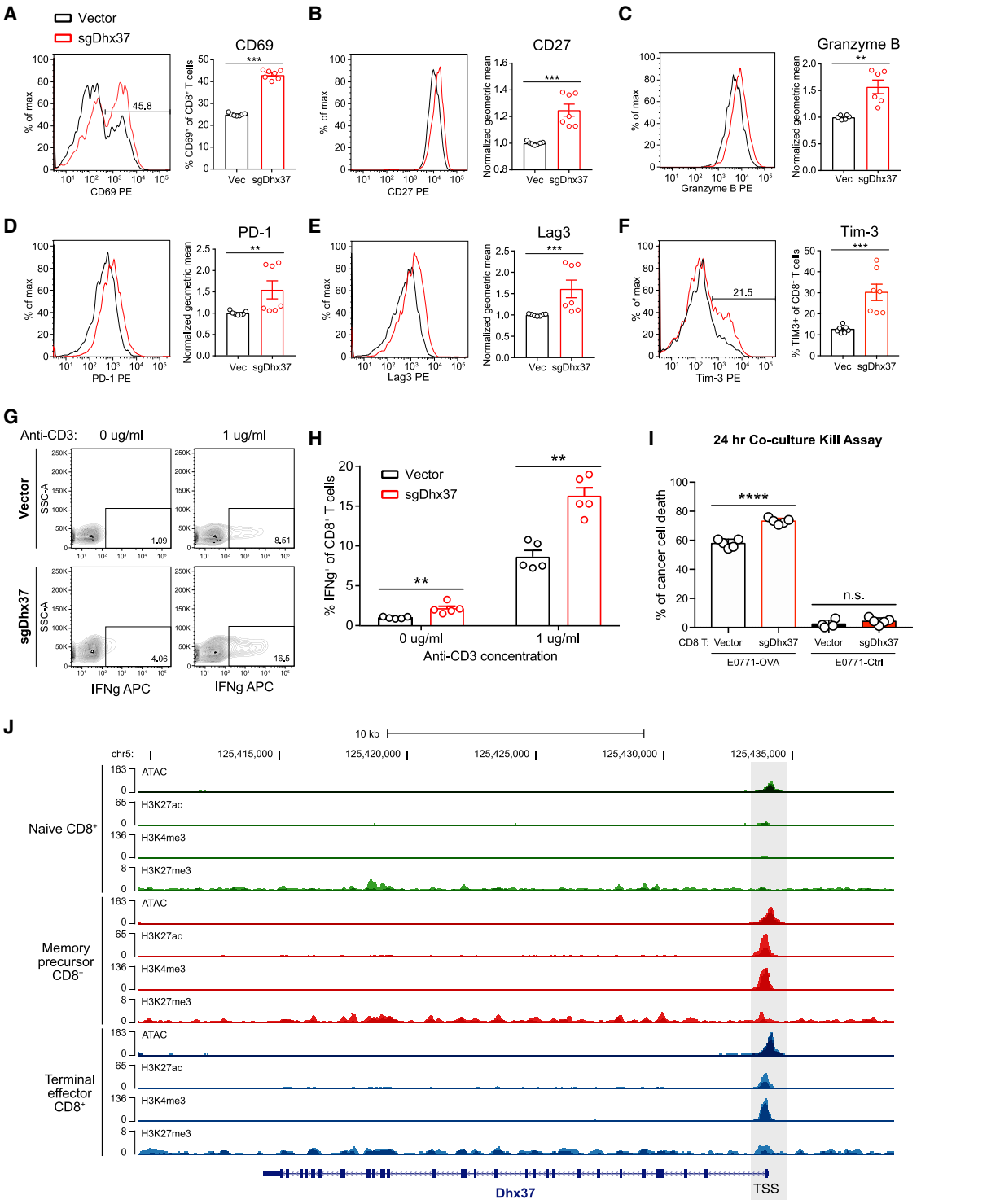


**Figure 5. Immunological Characterization of *Dhx37* Knockout Mouse CD8 T Cells**

(A–F) Flow cytometry analysis of key immune markers of T cell function, including CD69 (A), CD27 (B), Granzyme B (C), PD-1 (D), Lag3 (E), and Tim-3 (F). Left panel in each plot is a representative histogram of sgDhx37 (red) and vector (black) $CD8^+$ T cells. Right panel is a bar plot of quantification for each marker. Data are shown as mean ± SEM. *$p < 0.05$, **$p < 0.01$, ***$p < 0.001$, by unpaired two-sided Mann-Whitney test.

(G) Flow cytometry analysis plot of IFN-γ production of sgDhx37 and Vector CD8 T cells with or without anti-CD3 stimulation.

(H) Quantification bar plot of (G). Data are shown as mean ± SEM. **$p < 0.01$, by unpaired two-sided Mann-Whitney test.

*(legend continued on next page)*

the long-term *in vivo* tumor growth (6.5 week time course), we observed antigen decrease (Figures S4B–S4D), decrease of effective TILs (Figures S4F–S4H), and loss of T cell stimulation ability in cancer cells (Figures S5A–S5D), which is consistent with the current model of cancer immunoediting that might partly explain the ultimate rebound of tumors after adoptive transfer (Figure 2G and Figure 4I). These data validated that acute genetic perturbation of *Dhx37* led to enhanced killing by CD8 T cells, both *in vitro* and *in vivo*, together further validating the screen results.

We then characterized the immunological features of *Dhx37* mutant CD8 T cells. We found that *Dhx37* mutant CD8 T cells have higher levels of an activation marker CD69, as well as a co-stimulatory receptor CD27 (Figures 5A and 5B). Concordantly, *Dhx37* mutant cells produced higher level of granzyme B (Figure 5C). In line with the TIL scRNA-seq result, *Dhx37* mutant have higher levels of surface PD-1, Lag3, and Tim-3 (Figures 5D–5F), which are known immune checkpoints and also linked to intrinsic T cell activation (Lee et al., 2011). We then measured the ability of *Dhx37* mutant T cell's ability to produce IFN-γ, a major effector cytokine, and found that *Dhx37* mutant produced higher level of IFN-γ both at baseline and upon 1 μg/mL anti-CD3 stimulation (Figures 5G and 5H). In a co-culture assay, we found that *Dhx37* mutant (AAV-sgDhx37 treated) CD8 T cells are more potent in killing E0771-mCh-OVA cancer cell as compared to wild-type (vector treated) T cells (Figure 5I). The enhanced killing does not occur in parental E0771 cells without OVA, indicating that the effect is antigen specific (Figure 5I). By examining the epigenetic status of the *Dhx37* locus, we also found that memory precursor and terminal effector CD8 T cells have high levels of chromatin accessibility (assay for transposase-accessible chromatin using sequencing [ATAC-seq] peaks), promoter activity (H3K4me3) and enhancer activity (H3K27ac), while naive CD8 T cells have low levels of these markers (Figure 5J). These data together link *Dhx37* to T cell activation and effector function.

Of note, we also performed AAV-mediated gene editing and immunological assays for *Odc1* (Figures S6A and S6B; Table S3). We found that *Odc1* mutant T cells were able to degranulate in higher abundance in response to 1 ng/μL of SIINFEKL-pulsed E0771 cells compared to vector controls (Figures S6C and S6D). However, this increased responsiveness was not observed at a saturating dose of SIINFEKL peptide (10 ng/μL) (Figures S6C and S6D). Moreover, we revealed that *Odc1* mutant T cells also as showed increased effector functions in terms of granzyme and IFN-γ production (Figures S6E–S6G) as well as higher levels of CD69, CD27, PD-1, Lag3, and Tim-3 (Figure S6G).

## Bulk Transcriptome Profiling of *Dhx37* Mutant CD8 T Cells Revealed Immunologic Signatures of T Cell Activation and Effector Function along an NF-κB Axis

To identify genes downstream of *Dhx37*, we performed transcriptome profiling of *Dhx37* mutant CD8 T cells as compared to control T cells, using bulk mRNA-seq with 4 experimental replicates each (STAR Methods) (Table S4). We found a total of 97 significantly upregulated genes in *Dhx37* mutant CD8 T cells (sgDhx37 high genes) and 69 downregulated genes (sgDhx37 low genes) (Figure 6A) (Table S5). Consistent with the immune phenotyping results, among the *Dhx37* mutant upregulated genes are genes encoding effector cytokines such as various granzymes and IFN-γ, *Cd69*, *Tim-3* (*Havcr2*), and other immune genes *Serpinb6b* and *Serpinb9b* (Figure 6B). Examples of genes downregulated upon *Dhx37* loss include *Foxp3*, *Il6ra*, *Lyz2*, and *Ly6c2* (Figure 6B). We validated 5 individual genes by single-gene qPCR, and confirmed that all 5, i.e., *Gzmc*, *Gzmd*, *Sepinb9b*, *Tim-3*, and *Il6ra*, are differentially expressed (Figure 6C).

Because there are no existing studies of *Dhx37* perturbation in T cells, we compared the differential expression signatures to the expression profiles of naive, memory, and effector T cells, as well as effector cells under induced activation. We found that the upregulated gene set in *Dhx37* mutant is enriched in genes associated with T cell activation (Figure 6D; Table S6). We also found that the downregulated gene set is depleted in effector genes as compared to naive or memory T cells (Figure 6E; Table S6). Furthermore, DAVID pathway analysis (STAR Methods) revealed that the top two enriched pathways are immune response and cytolysis for *Dhx37* mutant upregulated gene set (Figure 6F), with the next tier of significant terms being inflammatory response, cell-surface protein, and extracellular exosome (Table S6). These analyses further linked *Dhx37* to T cell activation and effector function. Interestingly, when we examined the regulatory sequences in the promoters of genes upregulated upon *Dhx37* loss, the strongest sequence motif corresponded to the NF-κB motif (p = 1.053e-5) (Figure 6G), suggesting that Dhx37 may act, at least in part, through NF-κB components.

## Characterization of DHX37 in Human T Cells

Human *DHX37* encodes a 1,150 amino acid protein with several conserved domains, including the DEAH box (DEXDc), HrpA, NTPase, H2A, and the helicase (HELICc) domains (Figure S7A). Sequence alignment of DHX37 homologs from 32 species showed that this protein is highly conserved, especially in the DEXDc and helicase domains (Figure S7A). We made N- and C-terminal reporter fusion constructs and used them together with endogenous anti-DHX37 antibody to perform staining and imaging (STAR Methods). We found that both exogenous GFP-DHX37 and DHX37-GFP fusions overlap with those of the endogenous DHX37 protein, and they localize in nucleoli (Figures S7B and S7C). By western blot, we found that DHX37 protein is expressed in primary human $CD4^+$ and $CD8^+$ T cells, as well as patient TILs (Figure 7A). Based on the transcriptomic signature, pathway analysis, and motif analysis, we hypothesized that DHX37 interacts with NF-κB components. We performed immunoprecipitation (IP) on endogenous DHX37 protein with lysate

(I) Co-culture luciferase assay that measures the ability of sgDhx37 and Vector-treated CD8 T cells to kill antigen-expressing (E0771-OVA) and parental control (E0771-Ctrl) cells. Data are shown as mean ± SEM. ****p < 0.0001, by unpaired two-sided t test.

(J) Normalized signal tracks of ATAC-seq, H3K27ac, H3K4me3, and H3K27me3 chromatin immunoprecipitation sequencing (ChIP-seq) at the *Dhx37* locus in naive, memory precursor, and terminal effector $CD8^+$ T cells.

See also Figure S6.

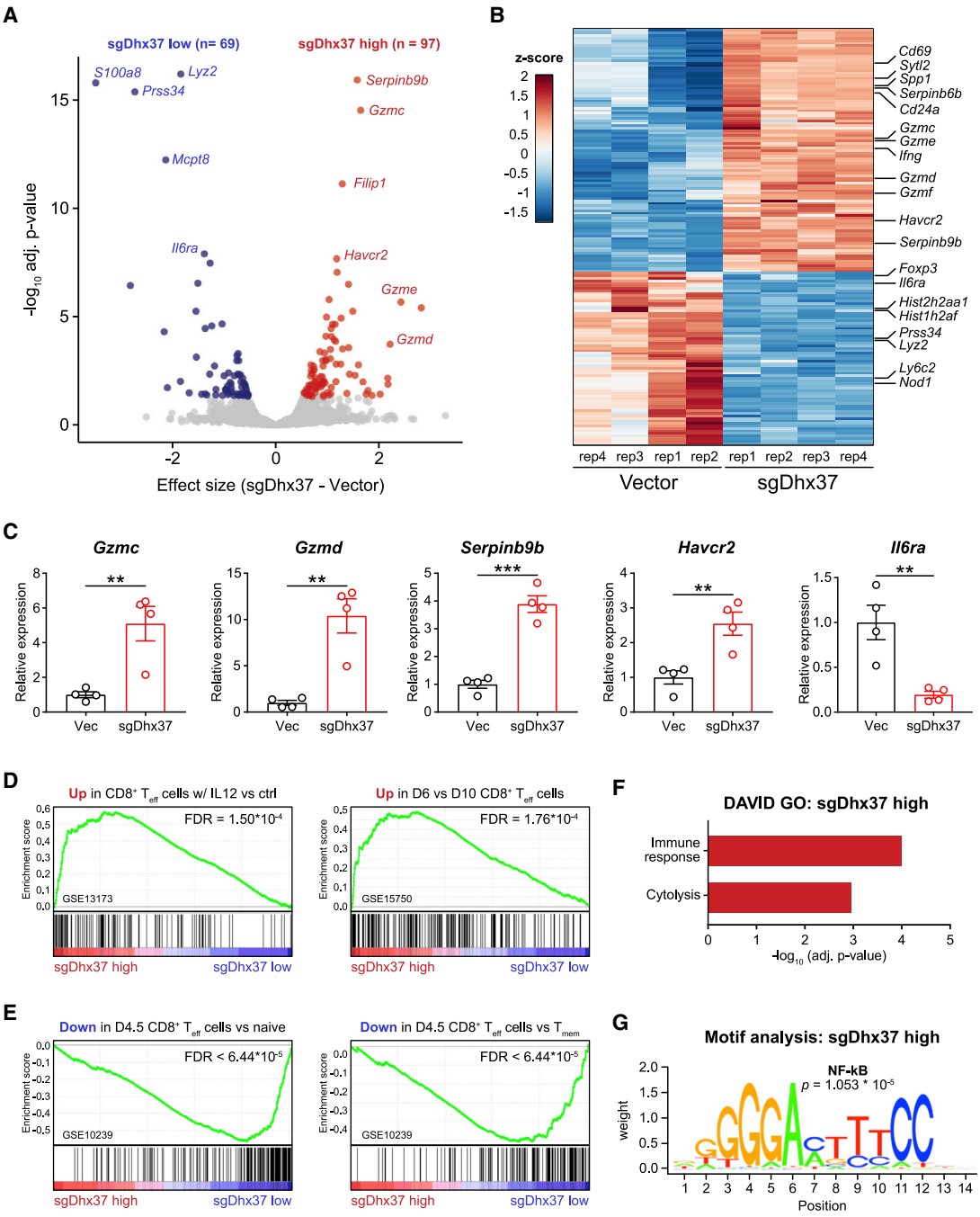


**Figure 6. Transcriptome Analysis of *Dhx37* Knockout Mouse CD8 T Cells by mRNA-Seq**

(A) Volcano plot of differentially expressed genes between *Dhx37* knockout and Vector control CD8 T cells, as quantified by bulk mRNA-seq (n = 4 biological replicates each).

(B) Heatmap of differentially mRNA-seq expressed genes in between *Dhx37* knockout and Vector control CD8 T cells.

(C) qPCR single-gene validation of representative highly upregulated or downregulated genes, including *Gzmc*, *Gzmd*, *Serpinb9b*, *Tim-3*, and *Il6ra*. Data are shown as mean ± SEM. *p < 0.05, **p < 0.01, ***p < 0.001, by unpaired two-sided t test.

(D and E) GSEA analysis of differentially expressed (DE) genes in *Dhx37* knockout CD8 T cells in known T effector signatures. (D) Analysis of *Dhx37-DE* upregulated gene set in (left) gene signature of IL-12 treatment versus control T effector cell and in (right) D6 versus D12 T effector cell in culture. (E) Analysis of *Dhx37-DE* downregulated gene set in (left) gene signature of effector versus naive CD8 T cell and in (right) effector versus memory CD8 T cell.

(F) DAVID GO analysis of *Dhx37-DE* upregulated gene set.

(G) Motif analysis of the regulatory DNA elements of the *Dhx37-DE* upregulated gene set, identifying the consensus NF-κB binding site as the top enriched motif.

See also Tables S4, S5, S6.

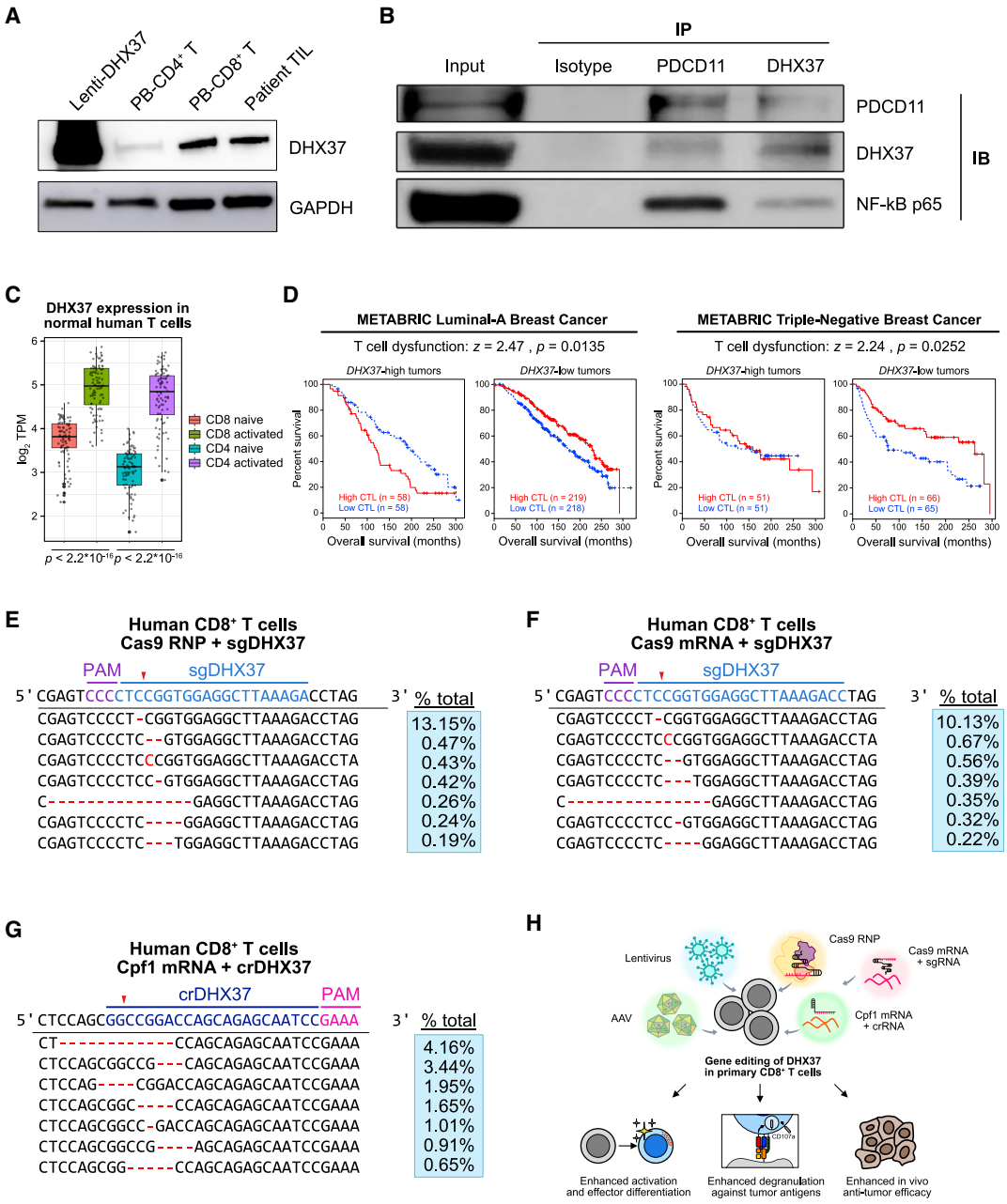


**Figure 7. Characterization of DHX37 in Human T Cells**

(A) Western blot analysis of DHX37 protein in human cells. From left to right, HEK293FT cells with *DHX37* cDNA overexpression as a positive control; peripheral blood CD4$^+$ T cells from a healthy donor; peripheral blood CD8$^+$ T cells from a healthy donor; TILs from a tumor biopsy freshly isolated from an non-small-cell lung carcinoma (NSCLC) patient.

(B) CoIP western experiment of DHX37 and NF-κB pathway components (PDCD11 and p65) in human primary CD8 T cells. Anti-DHX37 and Anti-PDCD11 reciprocal IPs were blotted with endogenous antibody against PDCD11, DHX37, and also along with p65.

(C) *DHX37* mRNA expression in normal human CD8$^+$ and CD4$^+$ T cells in activated and naive states. Statistical comparisons were made with two-sided unpaired Mann-Whitney test.

(D) TIDE analyses of *DHX37* expression in T cell dysfunction signatures linked to survival benefits in patients, with luminal-A or TNBC.

(E–G) Gene editing of the *DHX37* locus in primary human CD8 T cells, with Cas9 RNP (E), Cas9 mRNA (F), or Cpf1 mRNA (G) systems. Representative Illumina targeted amplicon sequencing of the sgRNA target site. Top most frequent variants were shown, with the associated variant frequencies in the box to the right. PAM and sgRNA spacers were indicated above. Red arrows indicate predicted cleavage sites. Red dashed lines indicate deletions. Red A/C/G/T where applicable indicate insertions.

(H) Schematics summarizing DHX37 targeting.

See also Figure S7 and Table S3.

from primary human CD8 T cells. We found that the NF-κB binding protein (PDCD11) and the NF-κB transcription factor p65 were detected in the DHX37-IP from CD8 T cell lysate (Figure 7B). We then performed a reciprocal IP with anti-PDCD11 antibody and detected both p65 and DHX37 in the PDCD11-IP fraction (Figure 7B).

Human *DHX37* is expressed in most organs, with highest expression in lymphoid tissues such as the bone marrow, lymph nodes, spleen, and appendix (Fagerberg et al., 2014). By analyzing *DHX37* expression in normal human T cells according to activation state, we found that activated T cells, both $CD8^+$ and $CD4^+$, have higher levels of *DHX37* (Figure 7C). By analyzing scRNA-seq data of human $CD8^+$ TILs from cancer patients, we found that *DHX37* is expressed at higher level in exhausted TILs compared to non-exhausted (Figure S7D). To examine the relevant roles of DHX37 in human T cells, we further analyzed a recent single-cell transcriptomics dataset of human TILs (Zheng et al., 2017a). *DHX37* mRNA expression was detected in a fraction of peripheral blood T cells, tissue-resident T cells, and tumor-infiltrating T cells (Figure S7E). *DHX37* was expressed in $CD3^+/CD8^+$ (cytotoxic T cell), $CD3^+/CD4^+/CD25^-$ (T helper cell), and $CD3^+/CD4^+/CD25^+$ (Treg) populations (Figure S7E), in those T cells from peripheral blood, resident tissue, tumor-normal junction, or infiltrated in the tumor (Figure S7E). To assess the clinical relevance of DHX37 in cancer, we used Tumor Immune Dysfunction and Exclusion (TIDE) analysis to examine whether *DHX37* expression in T cells is linked to breast cancer outcomes (STAR Methods). While high cytotoxic T lymphocyte (CTL) score is associated with an overall survival benefit, high-level of *DHX37* expression abolishes or negates this benefit, in both luminal-A and TNBC subtypes (Figure 7D). Together, these data showed that DHX37 is expressed in normal and tumor-associated human T cells, interacts with NF-κB core components, and is associated with T cell dysfunction related clinical outcomes in breast cancer patients.

## DISCUSSION

Tumor-derived TILs possess the ability to recognize and kill cancer cells in autologous transplantation studies (Rosenberg et al., 1985). The discovery of CTLA-4 and PD-1 pathways revealed how inhibitory signals of CD8 T cells can be exploited by tumors to evade immune recognition (Ishida et al., 1992; Leach et al., 1996). Targeting T cell inhibitory factors has led to the paradigm of checkpoint blockade immunotherapy (Fesnak et al., 2016; Maude et al., 2014; Maus and June, 2016; Mellman et al., 2011; Ribas, 2012), suggesting that better understanding of the genetic landscape governing T cell function will facilitate the development of better immunotherapies. CRISPR technology has provided a set of tools to open unique opportunities for direct manipulation of the T cell genome (Eyquem et al., 2017), and its scalability enabled genetic screens in T cells, which to date have been performed *in vitro* (Henriksson et al., 2019; Shifrut et al., 2018). Here, we performed convergent *in vivo* tumor infiltration and *in vitro* degranulation screens to systematically study the anti-tumor potential of CD8 T cells. Our screens generated genome-scale quantitative measurements of genetic factors modulating CD8 T cell phenotypes directly in immunotherapy-relevant settings, and identified enriched targets of various functional categories including known and undocumented.

A particularly exciting aspect of the infiltration screen is that, unlike other screens to date, PD-1 and Tim-3 emerged as top hits in an unbiased manner. These markers highlight the sensitivity of the *in vivo* screen in physiologically relevant conditions. This study can also serve as a reference for high-throughput genetic interrogation of T cells *in vivo* for immunotherapy target discovery. Possible alternative applications include a variety of cancer models such as genetically engineered mouse models as well as genome-editing based cancer models for diverse oncology indications, with or without other treatments in conjunction. Other CRISPR technologies such as CRISPR activation or repression, other vector or screening systems, and orthogonal genetic manipulation strategies may further empower the study of cancer immunotherapy with available and evolving toolkits (Dominguez et al., 2016; Esvelt et al., 2013; Gilbert et al., 2013; Thakore et al., 2016).

Validation and characterization of a top convergent hit, *Dhx37*, showed that modulation of this gene in CD8 T cells can lead to enhanced anti-tumor activity *in vitro* and *in vivo* by adoptive transfer. Due to the current lack of available compounds targeting DHX37, we reasoned that genetically editing *DHX37* in human CD8 T cells presented an approach for attenuating its activity. We performed ribonucleoprotein (RNP)-mediated and mRNA-mediated editing of *DHX37* in human CD8 T cells, using both Cas9 (Figures 7E and 7F; Table S3), and Cas12a-Cpf1 (Figure 7G; Table S3) systems. Multiple modes of delivery can be applied, including lentivirus, AAV, RNP, or mRNA (Figure 7H). Future studies may develop compounds targeting DHX37 by screening small molecule libraries or may use structure-based drug design.

## STAR★METHODS

Detailed methods are provided in the online version of this paper and include the following:

- KEY RESOURCES TABLE
- LEAD CONTACT AND MATERIALS AVAILABILITY
- EXPERIMENTAL MODEL AND SUBJECT DETAILS
  - Mice
- METHOD DETAILS
  - Generation of a T cell CRISPR vector
  - Genome-scale mouse T cell CRISPR library cloning
  - Viral library production
  - T cell isolation and culture
  - T cell transduction, virus titration
  - Antibody and Flow Cytometry
  - Library-scale viral transduction of T cells
  - Adoptive transfer of viral library infected T cells
  - Generation of a model antigen expression vector
  - Generation of mCherry-OVA cell line
  - Tumor transplantation and tissue processing
  - Antigen specificity testing for OT-I T cells
  - Degranulation screen and validation
  - Genomic DNA extraction

## SUPPLEMENTAL INFORMATION

Supplemental Information can be found online at https://doi.org/10.1016/j.cell.2019.07.044.

## ACKNOWLEDGMENTS

We thank all members of the Chen laboratory, as well as various colleagues in the Department of Genetics, Systems Biology Institute, Immunobiology Program, BBS Program, Cancer Center and Stem Cell Center at Yale for assistance and/or discussion. We thank the Center for Genome Analysis, Center for Molecular Discovery, Pathology Tissue Services, Histology Services, High Performance Computing Center, West Campus Analytical Chemistry Core and West Campus Imaging Core, and Keck Biotechnology Resource Laboratory at Yale for technical support. S.C. is supported by Yale SBI/Genetics Startup Fund, NIH/NCI (DP2CA238295-01, R01CA231112-01, R33CA225498-01A1, RF1DA048811, U54CA209992-8697, P50CA196530-A10805, P50CA121974-A08306), Damon Runyon Dale Frey Award (DFS-13-15), Melanoma Research Alliance (412806, 16-003524), St-Baldrick's Foundation (426685), Breast Cancer Alliance, Cancer Research Institute (CLIP), AACR (499395, 17-20-01-CHEN), The Mary Kay Foundation (017-81), The V Foundation (V2017-022), Ludwig Family Foundation, DoD (W81XWH-17-1-0235), Sontag Foundation (Chen DSA), and Chenevert Family Foundation. R.S.H. is supported by Yale SPORE in Lung Cancer (P50CA196530). M.B.D., R.D.C., and J.J.P. are supported by the Yale MSTP training grant from NIH (T32GM007205). C.D.G. and P.R. are supported by Yale PhD training grant from NIH (T32GM007499). G.W. is supported by CRI Irvington and RJ Anderson Postdoctoral Fellowships. X.D. is supported by a C Revson Postdoctoral Fellowship.

## AUTHOR CONTRIBUTIONS

S.C. and M.B.D. conceived, designed, and initiated the study. M.B.D. and S.C. generated T cell lentiCRISPR vectors and libraries. S.C., M.B.D., and G.W. generated relevant mouse strains. L.Y. generated T cell AAV-CRISPR system. M.B.D., G.W., and L.Y. performed most *in vivo* experiments. M.B.D. performed *in vitro* T cell immunology assays. R.D.C., J.J.P., and S.C. analyzed CRISPR screen data. R.D.C. analyzed mRNA-seq, single-cell, and immunogenomics data. L.Z. performed biochemistry experiments. X.D. isolated patient TILs and assisted human T cell experiments. H.R.K. assisted MD for various experiments. Y.E. performed histology experiments. C.D.G. assisted T cell library and sgRNA cloning. K.Y.C., X.Z., P.R., Y.D., J.S., S.Z.L., and J.J.Z. assisted parts of experiments. D.R.L. and R.S.H. provided clinical insights and patient samples for analysis. M.B.D., R.D.C., and S.C. jointly prepared the manuscript with inputs from all authors. S.C. secured funding and supervised the work.

## DECLARATION OF INTERESTS

R.S.H. is a consultant/advisory board member for Abbvie Pharmaceuticals, AstraZeneca, Biodesix, Bristol-Myers Squibb, Eli Lilly and Company, EMD Serrano, Genentech/Roche, Heat Biologics, Infinity Pharmaceuticals, Junshi Pharmaceuticals, Loxo Oncology, Merck and Company, Nektar, Neon Therapeutics, NextCure, Novartis, Pfizer, Sanofi, Seattle Genetics, Shire PLC, Spectrum Pharmaceuticals, Symphogen, and TESARO; has sponsored research grants from AstraZeneca, Eli Lilly and Company, and Merck and Company; and is a board member (non-executive/independent) for Junshi Pharmaceuticals. Yale filed a patent application related to the data described in this study.

Received: April 12, 2018
Revised: May 17, 2019
Accepted: July 24, 2019
Published: August 22, 2019

## REFERENCES

Abdelhaleem, M. (2005). RNA helicases: regulators of differentiation. Clin. Biochem. *38*, 499–503.

Alfei, F., Kanev, K., Hofmann, M., Wu, M., Ghoneim, H.E., Roelli, P., Utzschneider, D.T., von Hoesslin, M., Cullen, J.G., Fan, Y., et al. (2019). TOX reinforces the phenotype and longevity of exhausted T cells in chronic viral infection. Nature *571*, 265–269.

Beil-Wagner, J., Dössinger, G., Schober, K., vom Berg, J., Tresch, A., Grandl, M., Palle, P., Mair, F., Gerhard, M., Becher, B., et al. (2016). T cell-specific inactivation of mouse CD2 by CRISPR/Cas9. Sci. Rep. *6*, 21377.

Betts, M.R., Brenchley, J.M., Price, D.A., De Rosa, S.C., Douek, D.C., Roederer, M., and Koup, R.A. (2003). Sensitive and viable identification of antigen-specific CD8+ T cells by a flow cytometric assay for degranulation. J. Immunol. Methods *281*, 65–78.

Blankenstein, T., Coulie, P.G., Gilboa, E., and Jaffee, E.M. (2012). The determinants of tumour immunogenicity. Nat. Rev. Cancer *12*, 307–313.

Blum, J.S., Wearsch, P.A., and Cresswell, P. (2013). Pathways of antigen processing. Annu. Rev. Immunol. *31*, 443–473.

Brahmer, J.R., Drake, C.G., Wollner, I., Powderly, J.D., Picus, J., Sharfman, W.H., Stankevich, E., Pons, A., Salay, T.M., McMiller, T.L., et al. (2010). Phase I study of single-agent anti-programmed death-1 (MDX-1106) in refractory

solid tumors: safety, clinical activity, pharmacodynamics, and immunologic correlates. J. Clin. Oncol. *28*, 3167–3175.

Bray, N.L., Pimentel, H., Melsted, P., and Pachter, L. (2016). Near-optimal probabilistic RNA-seq quantification. Nat. Biotechnol. *34*, 525–527.

Butler, A., Hoffman, P., Smibert, P., Papalexi, E., and Satija, R. (2018). Integrating single-cell transcriptomic data across different conditions, technologies, and species. Nat. Biotechnol. *36*, 411–420.

Chen, D.S., and Mellman, I. (2013). Oncology meets immunology: the cancer-immunity cycle. Immunity *39*, 1–10.

Chen, J., López-Moyado, I.F., Seo, H., Lio, C.J., Hempleman, L.J., Sekiya, T., Yoshimura, A., Scott-Browne, J.P., and Rao, A. (2019). NR4A transcription factors limit CAR T cell function in solid tumours. Nature *567*, 530–534.

Chen, R., Bélanger, S., Frederick, M.A., Li, B., Johnston, R.J., Xiao, N., Liu, Y.C., Sharma, S., Peters, B., Rao, A., et al. (2014). In vivo RNA interference screens identify regulators of antiviral CD4(+) and CD8(+) T cell differentiation. Immunity *41*, 325–338.

Chia, J., Yeo, K.P., Whisstock, J.C., Dunstone, M.A., Trapani, J.A., and Voskoboinik, I. (2009). Temperature sensitivity of human perforin mutants unmasks subtotal loss of cytotoxicity, delayed FHL, and a predisposition to cancer. Proc. Natl. Acad. Sci. USA *106*, 9809–9814.

Chu, V.T., Weber, T., Graf, R., Sommermann, T., Petsch, K., Sack, U., Volchkov, P., Rajewsky, K., and Kühn, R. (2016). Efficient generation of Rosa26 knock-in mice using CRISPR/Cas9 in C57BL/6 zygotes. BMC Biotechnol. *16*, 4.

Clementi, R., Locatelli, F., Dupré, L., Garaventa, A., Emmi, L., Bregni, M., Cefalo, G., Moretta, A., Danesino, C., Comis, M., et al. (2005). A proportion of patients with lymphoma may harbor mutations of the perforin gene. Blood *105*, 4424–4428.

Cong, L., Ran, F.A., Cox, D., Lin, S., Barretto, R., Habib, N., Hsu, P.D., Wu, X., Jiang, W., Marraffini, L.A., and Zhang, F. (2013). Multiplex genome engineering using CRISPR/Cas systems. Science *339*, 819–823.

Cox, M.A., Harrington, L.E., and Zajac, A.J. (2011). Cytokines and the inception of CD8 T cell responses. Trends Immunol. *32*, 180–186.

Dai, X., Park, J.J., Du, Y., Kim, H.R., Wang, G., Errami, Y., and Chen, S. (2019). One-step generation of modular CAR-T cells with AAV-Cpf1. Nat. Methods *16*, 247–254.

Dominguez, A.A., Lim, W.A., and Qi, L.S. (2016). Beyond editing: repurposing CRISPR-Cas9 for precision genome regulation and interrogation. Nat. Rev. Mol. Cell Biol. *17*, 5–15.

Dumontet, E., Osman, J., Guillemont-Lambert, N., Cros, G., Moshous, D., and Picard, C. (2015). Recurrent Respiratory Infections Revealing CD8α Deficiency. J. Clin. Immunol. *35*, 692–695.

Esensten, J.H., Bluestone, J.A., and Lim, W.A. (2016). Engineering Therapeutic T Cells: From Synthetic Biology to Clinical Trials. Annu. Rev. Pathol. *12*, 305–330.

Esvelt, K.M., Mali, P., Braff, J.L., Moosburner, M., Yaung, S.J., and Church, G.M. (2013). Orthogonal Cas9 proteins for RNA-guided gene regulation and editing. Nat. Methods *10*, 1116–1121.

Eyquem, J., Mansilla-Soto, J., Giavridis, T., van der Stegen, S.J., Hamieh, M., Cunanan, K.M., Odak, A., Gönen, M., and Sadelain, M. (2017). Targeting a CAR to the TRAC locus with CRISPR/Cas9 enhances tumour rejection. Nature *543*, 113–117.

Fagerberg, L., Hallström, B.M., Oksvold, P., Kampf, C., Djureinovic, D., Odeberg, J., Habuka, M., Tahmasebpoor, S., Danielsson, A., Edlund, K., et al. (2014). Analysis of the human tissue-specific expression by genome-wide integration of transcriptomics and antibody-based proteomics. Mol. Cell. Proteomics *13*, 397–406.

Fesnak, A.D., June, C.H., and Levine, B.L. (2016). Engineered T cells: the promise and challenges of cancer immunotherapy. Nat. Rev. Cancer *16*, 566–581.

Fridman, W.H., Pagès, F., Sautès-Fridman, C., and Galon, J. (2012). The immune contexture in human tumours: impact on clinical outcome. Nat. Rev. Cancer *12*, 298–306.

Gaujoux, R., and Seoighe, C. (2010). A flexible R package for nonnegative matrix factorization. BMC Bioinformatics *11*, 367.

Ghoneim, H.E., Zamora, A.E., Thomas, P.G., and Youngblood, B.A. (2016). Cell-Intrinsic Barriers of T Cell-Based Immunotherapy. Trends Mol. Med. *22*, 1000–1011.

Gilbert, L.A., Larson, M.H., Morsut, L., Liu, Z., Brar, G.A., Torres, S.E., Stern-Ginossar, N., Brandman, O., Whitehead, E.H., Doudna, J.A., et al. (2013). CRISPR-mediated modular RNA-guided regulation of transcription in eukaryotes. Cell *154*, 442–451.

Gravano, D.M., and Hoyer, K.K. (2013). Promotion and prevention of autoimmune disease by CD8+ T cells. J. Autoimmun. *45*, 68–79.

Henriksson, J., Chen, X., Gomes, T., Ullah, U., Meyer, K.B., Miragaia, R., Duddy, G., Pramanik, J., Yusa, K., Lahesmaa, R., et al. (2019). Genome-wide CRISPR Screens in T Helper Cells Reveal Pervasive Crosstalk between Activation and Differentiation. Cell *176*, 882–896.

Hersperger, A.R., Martin, J.N., Shin, L.Y., Sheth, P.M., Kovacs, C.M., Cosma, G.L., Makedonas, G., Pereyra, F., Walker, B.D., Kaul, R., et al. (2011). Increased HIV-specific CD8+ T-cell cytotoxic potential in HIV elite controllers is associated with T-bet expression. Blood *117*, 3799–3808.

Hirata, H., Ogino, K., Yamada, K., Leacock, S., and Harvey, R.J. (2013). Defective escape behavior in DEAH-box RNA helicase mutants improved by restoring glycine receptor expression. J. Neurosci. *33*, 14638–14644.

Hogquist, K.A., Jameson, S.C., Heath, W.R., Howard, J.L., Bevan, M.J., and Carbone, F.R. (1994). T cell receptor antagonist peptides induce positive selection. Cell *76*, 17–27.

Holzelova, E., Vonarbourg, C., Stolzenberg, M.C., Arkwright, P.D., Selz, F., Prieur, A.M., Blanche, S., Bartunkova, J., Vilmer, E., Fischer, A., et al. (2004). Autoimmune lymphoproliferative syndrome with somatic Fas mutations. N. Engl. J. Med. *351*, 1409–1418.

Hsu, P.D., Lander, E.S., and Zhang, F. (2014). Development and applications of CRISPR-Cas9 for genome engineering. Cell *157*, 1262–1278.

Huang, W., Sherman, B.T., and Lempicki, R.A. (2009). Bioinformatics enrichment tools: paths toward the comprehensive functional analysis of large gene lists. Nucleic Acids Res. *37*, 1–13.

Ishida, Y., Agata, Y., Shibahara, K., and Honjo, T. (1992). Induced expression of PD-1, a novel member of the immunoglobulin gene superfamily, upon programmed cell death. EMBO J. *11*, 3887–3895.

Jackson, H.J., Rafiq, S., and Brentjens, R.J. (2016). Driving CAR T-cells forward. Nat. Rev. Clin. Oncol. *13*, 370–383.

Jiang, P., Gu, S., Pan, D., Fu, J., Sahu, A., Hu, X., Li, Z., Traugh, N., Bu, X., Li, B., et al. (2018). Signatures of T cell dysfunction and exclusion predict cancer immunotherapy response. Nat. Med. *10*, 1550–1558.

Jinek, M., Chylinski, K., Fonfara, I., Hauer, M., Doudna, J.A., and Charpentier, E. (2012). A programmable dual-RNA-guided DNA endonuclease in adaptive bacterial immunity. Science *337*, 816–821.

Johnson, L.A., and June, C.H. (2017). Driving gene-engineered T cell immunotherapy of cancer. Cell Res. *27*, 38–58.

Kaech, S.M., Wherry, E.J., and Ahmed, R. (2002). Effector and memory T-cell differentiation: implications for vaccine development. Nat. Rev. Immunol. *2*, 251–262.

Karaca, E., Harel, T., Pehlivan, D., Jhangiani, S.N., Gambin, T., Coban Akdemir, Z., Gonzaga-Jauregui, C., Erdin, S., Bayram, Y., Campbell, I.M., et al. (2015). Genes that Affect Brain Structure and Function Identified by Rare Variant Analyses of Mendelian Neurologic Disease. Neuron *88*, 499–513.

Kelderman, S., Schumacher, T.N., and Haanen, J.B. (2014). Acquired and intrinsic resistance in cancer immunotherapy. Mol. Oncol. *8*, 1132–1139.

Khan, O., Giles, J.R., McDonald, S., Manne, S., Ngiow, S.F., Patel, K.P., Werner, M.T., Huang, A.C., Alexander, K.A., Wu, J.E., et al. (2019). TOX transcriptionally and epigenetically programs $CD8^+$ T cell exhaustion. Nature *571*, 211–218.

Komor, A.C., Badran, A.H., and Liu, D.R. (2017). CRISPR-Based Technologies for the Manipulation of Eukaryotic Genomes. Cell *168*, 20–36.

Kurktschiev, P.D., Raziorrouh, B., Schraut, W., Backmund, M., Wächtler, M., Wendtner, C.M., Bengsch, B., Thimme, R., Denk, G., Zachoval, R., et al. (2014). Dysfunctional CD8+ T cells in hepatitis B and C are characterized by a lack of antigen-specific T-bet induction. J. Exp. Med. *211*, 2047–2059.

Kvistborg, P., Philips, D., Kelderman, S., Hageman, L., Ottensmeier, C., Joseph-Pietras, D., Welters, M.J., van der Burg, S., Kapiteijn, E., Michielin, O., et al. (2014). Anti-CTLA-4 therapy broadens the melanoma-reactive CD8+ T cell response. Sci. Transl. Med. *6*, 254ra128.

Langmead, B., Trapnell, C., Pop, M., and Salzberg, S.L. (2009). Ultrafast and memory-efficient alignment of short DNA sequences to the human genome. Genome Biol. *10*, R25.

Larkin, J., Chiarion-Sileni, V., Gonzalez, R., Grob, J.J., Cowey, C.L., Lao, C.D., Schadendorf, D., Dummer, R., Smylie, M., Rutkowski, P., et al. (2015). Combined Nivolumab and Ipilimumab or Monotherapy in Untreated Melanoma. N. Engl. J. Med. *373*, 23–34.

Laumont, C.M., Vincent, K., Hesnard, L., Audemard, É., Bonneil, É., Laverdure, J.P., Gendron, P., Courcelles, M., Hardy, M.P., Côté, C., et al. (2018). Noncoding regions are the main source of targetable tumor-specific antigens. Sci. Transl. Med. *10*. Published online December 5, 2019. https://doi.org/10.1126/scitranslmed.aau5516.

Leach, D.R., Krummel, M.F., and Allison, J.P. (1996). Enhancement of antitumor immunity by CTLA-4 blockade. Science *271*, 1734–1736.

Lee, J., Su, E.W., Zhu, C., Hainline, S., Phuah, J., Moroco, J.A., Smithgall, T.E., Kuchroo, V.K., and Kane, L.P. (2011). Phosphotyrosine-dependent coupling of Tim-3 to T-cell receptor signaling pathways. Mol. Cell. Biol. *31*, 3963–3974.

Li, W., Xu, H., Xiao, T., Cong, L., Love, M.I., Zhang, F., Irizarry, R.A., Liu, J.S., Brown, M., and Liu, X.S. (2014). MAGeCK enables robust identification of essential genes from genome-scale CRISPR/Cas9 knockout screens. Genome Biol. *15*, 554.

Lun, A.T., McCarthy, D.J., and Marioni, J.C. (2016). A step-by-step workflow for low-level analysis of single-cell RNA-seq data with Bioconductor. F1000Res. *5*, 2122.

Luo, B., Cheung, H.W., Subramanian, A., Sharifnia, T., Okamoto, M., Yang, X., Hinkle, G., Boehm, J.S., Beroukhim, R., Weir, B.A., et al. (2008). Highly parallel identification of essential genes in cancer cells. Proc. Natl. Acad. Sci. USA *105*, 20380–20385.

Mahoney, K.M., Rennert, P.D., and Freeman, G.J. (2015). Combination cancer immunotherapy and new immunomodulatory targets. Nat. Rev. Drug Discov. *14*, 561–584.

Mali, P., Yang, L., Esvelt, K.M., Aach, J., Guell, M., DiCarlo, J.E., Norville, J.E., and Church, G.M. (2013). RNA-guided human genome engineering via Cas9. Science *339*, 823–826.

Martin, M. (2011). Cutadapt removes adapter sequences from high-throughput sequencing reads. EMBnetjournal *17*, 10–12.

Maude, S.L., Frey, N., Shaw, P.A., Aplenc, R., Barrett, D.M., Bunin, N.J., Chew, A., Gonzalez, V.E., Zheng, Z., Lacey, S.F., et al. (2014). Chimeric antigen receptor T cells for sustained remissions in leukemia. N. Engl. J. Med. *371*, 1507–1517.

Maus, M.V., and June, C.H. (2016). Making Better Chimeric Antigen Receptors for Adoptive T-cell Therapy. Clin. Cancer Res. *22*, 1875–1884.

Mellman, I., Coukos, G., and Dranoff, G. (2011). Cancer immunotherapy comes of age. Nature *480*, 480–489.

Mi, H., Muruganujan, A., Casagrande, J.T., and Thomas, P.D. (2013). Large-scale gene function analysis with the PANTHER classification system. Nat. Protoc. *8*, 1551–1566.

Mombaerts, P., Iacomini, J., Johnson, R.S., Herrup, K., Tonegawa, S., and Papaioannou, V.E. (1992). RAG-1-deficient mice have no mature B and T lymphocytes. Cell *68*, 869–877.

Mortaz, E., Tabarsi, P., Mansouri, D., Khosravi, A., Garssen, J., Velayati, A., and Adcock, I.M. (2016). Cancers Related to Immunodeficiencies: Update and Perspectives. Front. Immunol. *7*, 365.

Nijman, S.M. (2015). Functional genomics to uncover drug mechanism of action. Nat. Chem. Biol. *11*, 942–948.

Pardoll, D.M. (2012). The blockade of immune checkpoints in cancer immunotherapy. Nat. Rev. Cancer *12*, 252–264.

Pimentel, H., Bray, N.L., Puente, S., Melsted, P., and Pachter, L. (2017). Differential analysis of RNA-seq incorporating quantification uncertainty. Nat. Methods *14*, 687–690.

Platt, R.J., Chen, S., Zhou, Y., Yim, M.J., Swiech, L., Kempton, H.R., Dahlman, J.E., Parnas, O., Eisenhaure, T.M., Jovanovic, M., et al. (2014). CRISPR-Cas9 knockin mice for genome editing and cancer modeling. Cell *159*, 440–455.

Porgador, A., Yewdell, J.W., Deng, Y., Bennink, J.R., and Germain, R.N. (1997). Localization, quantitation, and in situ detection of specific peptide-MHC class I complexes using a monoclonal antibody. Immunity *6*, 715–726.

Postow, M.A., Chesney, J., Pavlick, A.C., Robert, C., Grossmann, K., McDermott, D., Linette, G.P., Meyer, N., Giguere, J.K., Agarwala, S.S., et al. (2015). Nivolumab and ipilimumab versus ipilimumab in untreated melanoma. N. Engl. J. Med. *372*, 2006–2017.

Restifo, N.P., Smyth, M.J., and Snyder, A. (2016). Acquired resistance to immunotherapy and future challenges. Nat. Rev. Cancer *16*, 121–126.

Ribas, A. (2012). Tumor immunotherapy directed at PD-1. N. Engl. J. Med. *366*, 2517–2519.

Robinson, M.D., McCarthy, D.J., and Smyth, G.K. (2010). edgeR: a Bioconductor package for differential expression analysis of digital gene expression data. Bioinformatics *26*, 139–140.

Rosenberg, S.A., Lotze, M.T., Muul, L.M., Leitman, S., Chang, A.E., Ettinghausen, S.E., Matory, Y.L., Skibber, J.M., Shiloni, E., Vetto, J.T., et al. (1985). Observations on the systemic administration of autologous lymphokine-activated killer cells and recombinant interleukin-2 to patients with metastatic cancer. N. Engl. J. Med. *313*, 1485–1492.

Roychowdhury, A., Joret, C., Bourgeois, G., Heurgué-Hamard, V., Lafontaine, D.L.J., and Graille, M. (2019). The DEAH-box RNA helicase Dhr1 contains a remarkable carboxyl terminal domain essential for small ribosomal subunit biogenesis. Nucleic Acids Res., gkz529.

Sade-Feldman, M., Yizhak, K., Bjorgaard, S.L., Ray, J.P., de Boer, C.G., Jenkins, R.W., Lieb, D.J., Chen, J.H., Frederick, D.T., Barzily-Rokni, M., et al. (2018). Defining T Cell States Associated with Response to Checkpoint Immunotherapy in Melanoma. Cell *175*, 998–1013.

Sanjana, N.E., Shalem, O., and Zhang, F. (2014). Improved vectors and genome-wide libraries for CRISPR screening. Nat. Methods *11*, 783–784.

Schmiedel, B.J., Singh, D., Madrigal, A., Valdovino-Gonzalez, A.G., White, B.M., Zapardiel-Gonzalo, J., Ha, B., Altay, G., Greenbaum, J.A., McVicker, G., et al. (2018). Impact of Genetic Polymorphisms on Human Immune Cell Gene Expression. Cell *175*, 1701–1715.

Scott, A.C., Dündar, F., Zumbo, P., Chandran, S.S., Klebanoff, C.A., Shakiba, M., Trivedi, P., Menocal, L., Appleby, H., Camara, S., et al. (2019). TOX is a critical regulator of tumour-specific T cell differentiation. Nature *571*, 270–274.

Shalem, O., Sanjana, N.E., Hartenian, E., Shi, X., Scott, D.A., Mikkelson, T., Heckl, D., Ebert, B.L., Root, D.E., Doench, J.G., and Zhang, F. (2014). Genome-scale CRISPR-Cas9 knockout screening in human cells. Science *343*, 84–87.

Shalem, O., Sanjana, N.E., and Zhang, F. (2015). High-throughput functional genomics using CRISPR-Cas9. Nat. Rev. Genet. *16*, 299–311.

Sharon, E., Streicher, H., Goncalves, P., and Chen, H.X. (2014). Immune checkpoint inhibitors in clinical trials. Chin. J. Cancer *33*, 434–444.

Shifrut, E., Carnevale, J., Tobin, V., Roth, T.L., Woo, J.M., Bui, C.T., Li, P.J., Diolaiti, M.E., Ashworth, A., and Marson, A. (2018). Genome-wide CRISPR Screens in Primary Human T Cells Reveal Key Regulators of Immune Function. Cell *175*, 1958–1971.

Singer, M., Wang, C., Cong, L., Marjanovic, N.D., Kowalczyk, M.S., Zhang, H., Nyman, J., Sakuishi, K., Kurtulus, S., Gennert, D., et al. (2016). A Distinct Gene Module for Dysfunction Uncoupled from Activation in Tumor-Infiltrating T Cells. Cell *166*, 1500–1511.

Spranger, S., Spaapen, R.M., Zha, Y., Williams, J., Meng, Y., Ha, T.T., and Gajewski, T.F. (2013). Up-regulation of PD-L1, IDO, and T(regs) in the melanoma

tumor microenvironment is driven by CD8(+) T cells. Sci. Transl. Med. *5*, 200ra116.

Srivastava, S., and Riddell, S.R. (2015). Engineering CAR-T cells: Design concepts. Trends Immunol. *36*, 494–502.

Su, S., Hu, B., Shao, J., Shen, B., Du, J., Du, Y., Zhou, J., Yu, L., Zhang, L., Chen, F., et al. (2016). CRISPR-Cas9 mediated efficient PD-1 disruption on human primary T cells from cancer patients. Sci. Rep. *6*, 20070.

Subramanian, A., Tamayo, P., Mootha, V.K., Mukherjee, S., Ebert, B.L., Gillette, M.A., Paulovich, A., Pomeroy, S.L., Golub, T.R., Lander, E.S., and Mesirov, J.P. (2005). Gene set enrichment analysis: a knowledge-based approach for interpreting genome-wide expression profiles. Proc. Natl. Acad. Sci. USA *102*, 15545–15550.

Swart, M., Verbrugge, I., and Beltman, J.B. (2016). Combination Approaches with Immune-Checkpoint Blockade in Cancer Therapy. Front. Oncol. *6*, 233.

Thakore, P.I., Black, J.B., Hilton, I.B., and Gersbach, C.A. (2016). Editing the epigenome: technologies for programmable transcription and epigenetic modulation. Nat. Methods *13*, 127–137.

Tirosh, I., Izar, B., Prakadan, S.M., Wadsworth, M.H., 2nd, Treacy, D., Trombetta, J.J., Rotem, A., Rodman, C., Lian, C., Murphy, G., et al. (2016). Dissecting the multicellular ecosystem of metastatic melanoma by single-cell RNA-seq. Science *352*, 189–196.

Tsantikos, E., Quilici, C., Harder, K.W., Wang, B., Zhu, H.J., Anderson, G.P., Tarlinton, D.M., and Hibbs, M.L. (2009). Perturbation of the CD4 T cell compartment and expansion of regulatory T cells in autoimmune-prone Lyn-deficient mice. J. Immunol. *183*, 2484–2494.

Tscharke, D.C., Croft, N.P., Doherty, P.C., and La Gruta, N.L. (2015). Sizing up the key determinants of the CD8(+) T cell response. Nat. Rev. Immunol. *15*, 705–716.

Tumeh, P.C., Harview, C.L., Yearley, J.H., Shintaku, I.P., Taylor, E.J., Robert, L., Chmielowski, B., Spasic, M., Henry, G., Ciobanu, V., et al. (2014). PD-1 blockade induces responses by inhibiting adaptive immune resistance. Nature *515*, 568–571.

Valori, M., Jansson, L., Kiviharju, A., Ellonen, P., Rajala, H., Awad, S.A., Mustjoki, S., and Tienari, P.J. (2017). A novel class of somatic mutations in blood detected preferentially in CD8+ cells. Clin. Immunol. *175*, 75–81.

van der Maaten, L.J.P. (2014). Accelerating t-SNE using Tree-Based Algorithms. J. Machine Learning Res. *15*, 3221–3245.

van der Maaten, L.J.P., and Hinton, G.E. (2008). Visualizing High-Dimensional Data Using t-SNE. J. Machine Learning Res. *9*, 2579–2605.

Walter, U., and Santamaria, P. (2005). CD8+ T cells in autoimmunity. Curr. Opin. Immunol. *17*, 624–631.

Wang, T., Wei, J.J., Sabatini, D.M., and Lander, E.S. (2014). Genetic screens in human cells using the CRISPR-Cas9 system. Science *343*, 80–84.

Wong, P., and Pamer, E.G. (2003). CD8 T cell responses to infectious pathogens. Annu. Rev. Immunol. *21*, 29–70.

Wright, A.V., Nuñez, J.K., and Doudna, J.A. (2016). Biology and Applications of CRISPR Systems: Harnessing Nature's Toolbox for Genome Engineering. Cell *164*, 29–44.

Yamanashi, Y., Mori, S., Yoshida, M., Kishimoto, T., Inoue, K., Yamamoto, T., and Toyoshima, K. (1989). Selective expression of a protein-tyrosine kinase, p56lyn, in hematopoietic cells and association with production of human T-cell lymphotropic virus type I. Proc. Natl. Acad. Sci. USA *86*, 6538–6542.

Zambelli, F., Pesole, G., and Pavesi, G. (2009). Pscan: finding over-represented transcription factor binding site motifs in sequences from co-regulated or co-expressed genes. Nucleic Acids Res. *37*, W247–W252.

Zhang, N., and Bevan, M.J. (2011). CD8(+) T cells: foot soldiers of the immune system. Immunity *35*, 161–168.

Zhang, Q., Davis, J.C., Lamborn, I.T., Freeman, A.F., Jing, H., Favreau, A.J., Matthews, H.F., Davis, J., Turner, M.L., Uzel, G., et al. (2009). Combined immunodeficiency associated with DOCK8 mutations. N. Engl. J. Med. *361*, 2046–2055.

Zheng, C., Zheng, L., Yoo, J.K., Guo, H., Zhang, Y., Guo, X., Kang, B., Hu, R., Huang, J.Y., Zhang, Q., et al. (2017a). Landscape of Infiltrating T Cells in Liver Cancer Revealed by Single-Cell Sequencing. Cell *169*, 1342–1356.

Zheng, G.X., Terry, J.M., Belgrader, P., Ryvkin, P., Bent, Z.W., Wilson, R., Ziraldo, S.B., Wheeler, T.D., McDermott, G.P., Zhu, J., et al. (2017b). Massively parallel digital transcriptional profiling of single cells. Nat. Commun. *8*, 14049.

Zhou, P., Shaffer, D.R., Alvarez Arias, D.A., Nakazaki, Y., Pos, W., Torres, A.J., Cremasco, V., Dougan, S.K., Cowley, G.S., Elpek, K., et al. (2014). In vivo discovery of immunotherapy targets in the tumour microenvironment. Nature *506*, 52–57.

## STAR★METHODS

### KEY RESOURCES TABLE

| REAGENT or RESOURCE | SOURCE | IDENTIFIER |
|---|---|---|
| Antibodies | | |
| VeriBlot for IP Detection Reagent (HRP) | AbCam | Cat#ab131366-500ul |
| DHX37 Polyclonal Antibody | Bethyl | Cat#A300-856A; RRID:AB_2292875 |
| PDCD11 Polyclonal Antibody | Bethyl | Cat#A303805A; RRID:AB_11218382 |
| APC anti-human CD3 Antibody (Clone: HIT3a) | Biolegend | Cat#300312; RRID:AB_314048 |
| APC anti-mouse CD3ε Antibody (clone: 145-2C11) | Biolegend | Cat#100312; RRID:AB_312677 |
| APC anti-mouse IFN-γ Antibody (clone: XMG1.2) | Biolegend | Cat#505810; RRID:AB_315404 |
| FITC anti-mouse CD8a Antibody (clone: 53-6.7) | Biolegend | Cat#100706; RRID:AB_312745 |
| PE anti-human IgG Fc Antibody (clone: HP6017) | Biolegend | Cat#409304; RRID:AB_10895907 |
| PE anti-human/mouse Granzyme B Recombinant Antibody (clone: QA16A02) | Biolegend | Cat#372208; RRID:AB_2687032 |
| PE anti-mouse CD107a (LAMP-1) Antibody (clone: 1D4B) | Biolegend | Cat#121612; RRID:AB_2134487 |
| PE anti-mouse CD223 (LAG-3) Antibody (clone: C9B7W) | Biolegend | Cat#125208; RRID:AB_2133343 |
| PE anti-mouse CD279 (PD-1) Antibody (clone: 29F.1A12) | Biolegend | Cat#135206; RRID:AB_1877231 |
| PE anti-mouse CD366 (Tim-3) Antibody (clone: B8.2C12) | Biolegend | Cat#134003; RRID:AB_1626181 |
| PE anti-mouse CD62L Antibody (clone: MEL-14) | Biolegend | Cat#104408; RRID:AB_313095 |
| PE anti-mouse CD69 Antibody (clone: H1.2F3) | Biolegend | Cat#104508; RRID:AB_313111 |
| PE anti-mouse H-2Kb bound to SIINFEKL Antibody (clone: 25-D1.16) | Biolegend | Cat#141604; RRID:AB_10895905 |
| PE anti-mouse/human CD44 Antibody (clone: IM7) | Biolegend | Cat#103008; RRID:AB_312959 |
| PE anti-mouse/rat/human CD27 Antibody (clone: LG.3A10) | Biolegend | Cat#124210; RRID:AB_1236459 |
| PE anti-rat CD90/mouse CD90.1 (Thy-1.1) Antibody (clone: OX-7) | Biolegend | Cat#202524; RRID:AB_1595524 |
| PE/Cy7 anti-mouse CD3epsilon Antibody (clone: 145-2C11) | Biolegend | Cat#100320; RRID:AB_312685 |
| PerCP/Cy5.5 anti-mouse CD45.2 Antibody (clone: 104) | Biolegend | Cat#109828; RRID:AB_893350 |
| Ultra-LEAF Purified anti-mouse CD3ε Antibody (clone: 145-2C11) | Biolegend | Cat#100340; RRID:AB_11149115 |
| Ultra-LEAF(TM) Purified anti-mouse CD28 Antibody (clone: 37.51) | Biolegend | Cat#102116; RRID:AB_11147170 |
| Ultra-LEAF Purified anti-mouse CD16/32 Antibody (clone: 93) | Biolegend | Cat#101330; RRID:AB_2561482 |
| beta actin loading control (clone: BA3R) | Invitrogen | Cat#MA5-15739; RRID:AB_10979409 |
| Dynabeads Human T-Activator CD3/CD28 | Invitrogen | Cat#11131D |
| LIVE/DEAD Fixable Near-IR Dead Cell Stain Kit, for 633 or 635 nm excitation | Invitrogen | Cat#L34976 |
| NFkB p65 Antibody (4-2HCLC), ABfinity Rabbit Oligoclonal (lot:) | Invitrogen | Cat#710048; RRID:AB_2532539 |
| Rabbit polyclonal anti-human/mouse Dhx37 (Lot: R44921) | Novus | Cat#NBP2-13922 |
| GAPDH Antibody (clone: 6C5) | Santa Cruz | Cat#sc-32233; RRID:AB_627679 |
| anti-GFP | AbCam | Cat#ab290; RRID:AB_303395 |
| Anti-Nucleolin antibody | AbCam | Cat#ab22758; RRID:AB_776878 |
| Bacterial and Virus Strains | | |
| One Shot Stbl3 Chemical Competent *E. coli* | ThermoFisher | Cat#C737303 |
| Endura ElectroCompetent Cells | Lucigen | Cat#60242-2 |
| Chemicals, Peptides, and Recombinant Proteins | | |
| DPBS, no calcium, no magnesium | GIBCO | Cat#14190250 |
| RPMI 1640 Medium | GIBCO | Cat#11875-093 |
| DMEM, high glucose, pyruvate | GIBCO | Cat#11995065 |
| Fetal Bovine Serum | Sigma Aldrich | Cat#F4135-500ML |
| Penicillin-Streptomycin (10,000 U/mL) | GIBCO | Cat#15140122 |

(*Continued on next page*)

*Continued*

| REAGENT or RESOURCE | SOURCE | IDENTIFIER |
|---|---|---|
| Lonza BioWhittaker L-Glutamine (200mM) | Lonza | Cat#BW17605E |
| 2-Mercaptoethanol | Sigma Aldrich | Cat#M6250-10ML |
| X-VIVO 15 Serum-free Hematopoietic Cell Medium | Lonza | Cat#BE02-060F |
| Corning; Human AB Serum; Male Donors; type AB; US; 100mL, 35-060-CI 1/EA | Corning | Cat#MT35060CI |
| ACK Lysing Buffer | Lonza | Cat#10-548E |
| Naive CD8a+ T Cell Isolation Kit, mouse | Miltenyi | Cat#130-096-543 |
| LS Columns | Miltenyi | Cat#130-042-401 |
| Recombinant Mouse IL-2 (carrier-free) | Biolegend | Cat#575404 |
| Recombinant Mouse IL-7 (carrier-free) | Biolegend | Cat#577802 |
| Recombinant Mouse IL-12 (p70) (carrier-free) | Biolegend | Cat# |
| Recombinant Mouse IL-15 (carrier-free) | Biolegend | Cat#566302 |
| Recombinant Human IL-2 (carrier-free) | Biolegend | Cat#589104 |
| Dynabeads Human T-Activator CD3/CD28 | Invitrogen | Cat#11131D |
| Ficoll-Paque PLUS | GE Healthcare Life Sciences | Cat#17144002 |
| Collagenase IV | ThermoFisher | Cat#17104019 |
| OVA 257-264 | Invivogen | Cat#vac-sin |
| Monensin Solution (1,000x) | Biolegend | Cat#420701 |
| QuickExtract DNA Extraction Solution | Epicenter | Cat#QE09050 |
| QIAamp Fast DNA Tissue Kit | QIAGEN | Cat#51404 |
| T7 Endonuclease I | NEB | Cat#M0302L |
| Proteinase K | QIAGEN | Cat#19131 |
| RNase A | QIAGEN | Cat#19101 |
| Gibson Assembly Master Mix | NEB | Cat#E2611 |
| Phusion Flash High-Fidelity PCR Master Mix | ThermoFisher | Cat#F548L |
| DreamTaq Green PCR Master Mix (2X) | ThermoFisher | Cat#K1082 |
| QIAquick Gel Extraction Kit | QIAGEN | Cat#28706 |
| E-Gel Low Range Quantitative DNA Ladder | ThermoFisher | Cat#12373031 |
| Fixation/Permeabilization Solution Kit | BD | Cat#554714 |
| Nextera DNA Library Prep Kit | Illumina | Cat#FC-121-1030 |
| Nextera Index Kit | Illumina | Cat#FC-121-1011 |
| TRIzol Reagent | Invitrogen | Cat#15596026 |
| PureLink RNA Mini Kit | Invitrogen | Cat#12183018A |
| PureLink DNase Set | Invitrogen | Cat#12185010 |
| SuperScript IV Reverse Transcriptase | Invitrogen | Cat#18090050 |
| Random Hexamers (50 μM) | Invitrogen | Cat#N8080127 |
| TaqMan Fast Advanced Master Mix | Invitrogen | Cat#4444557 |
| BpiI (BbsI) (10 U/μL) | ThermoFisher | Cat#ER1012 |
| Esp3I (BsmBI) (10 U/μL) | ThermoFisher | Cat#ER0451 |
| Benzonase Nuclease | ThermoFisher | Cat#E1014-25KU |
| Dynabeads Protein A for Immunoprecipitation | Invitrogen | Cat#10002D |
| NuPAGE LDS Sample Buffer (4X) | Invitrogen | Cat#NP0008 |
| NuPAGE 3-8% Tris-Acetate Protein Gels, 1.5 mm, 10-well | Invitrogen | Cat#EA0378BOX |
| 4–20% Mini-PROTEAN TGX Precast Protein Gels, 10-well | BioRad | Cat#4561094 |
| Bovine Serum Albumin | Sigma Aldrich | Cat#A9418-100G |
| Pierce ECL Western Blotting Substrate | ThermoFisher | Cat#32106 |
| EDTA | Sigma Aldrich | Cat#E8008-100ML |

(*Continued on next page*)

*Continued*

| REAGENT or RESOURCE | SOURCE | IDENTIFIER |
|---|---|---|
| XenoLight D-Luciferin - K+ Salt Bioluminescent Substrate | Perkin Elmer | Cat#122799 |
| Neon Transfection System 100 μL Kit | Invitrogen | Cat#MPK10025 |
| Cas9 protein | IDT | Cat#1081058 |
| Cas9 mRNA | Trilink | Cat#L-7206 |
| Cpf1 mRNA | Trilink | Cat#L-7009 |
| Cas9 tracrRNA | IDT | Cat#1072532 |
| DHX37 crRNA (Cas9) | IDT | Custom, sequence specific |
| DHX37 crRNA (Cpf1) | Sigma | Custom, sequence specific |
| Critical Commercial Assays | | |
| Qubit dsDNA HS Assay Kit | ThermoFisher | Cat#Q32854 |
| Chromium Single Cell | 10x Genomics | V2 discontinued, alternative is v3, Cat#1000092 |
| Deposited Data | | |
| Human T cell single cell RNA-seq | Zheng et al., 2017a | GEO: GSE98638 |
| Dhx37 single cell RNaseq | This paper, GEO | GEO: GSE132960 |
| Dhx37 mRNaseq | This paper, GEO | GEO: GSE132960 |
| Dhx37 and Odc1 CRISPR Cas9 and Cas12a/Cpf1 mutagenesis indels | This paper, SRA | SRA: PRJNA549266 |
| qPCR data | This paper, Mendeley Data | https://doi.org/10.17632/2ffxmf3d7k.1 |
| Flow data | This paper, Mendeley Data | https://doi.org/10.17632/2ffxmf3d7k.1 |
| Experimental Models: Cell Lines | | |
| HEK293FT | ThermoFisher | Catalog Number: R70007 |
| E0771 | CH3 | Catalog Number: 940001 |
| Experimental Models: Organisms/Strains | | |
| OT-I | Jackson Laboratory | Catalog Number: 003831 |
| Cas9 | Chu et al., 2016; Platt et al., 2014 | Jackson Lab |
| OT-I;Cas9 | This paper | N/A |
| Rag1−/− | Jackson Laboratory | Catalog Number: 002216 |
| Oligonucleotides | | |
| guide RNA spacer oligos | This paper | Table S7 |
| amplicon primers for surveyor or Nextera | This paper | Table S7 |
| Recombinant DNA | | |
| MGC Mouse Dhx37 cDNA | Dharmacon | MMM1013-202797609 |
| DHX37-GFP | This paper | Addgene, N/A |
| GFP-DHX37 | This paper | Addgene, N/A |
| T cell LentiCRISPR vector (pSC008) | This paper | Addgene, N/A |
| T cell AAVCRISPR vector (pLY05) | This paper | Addgene, N/A |
| mGeCKOa | Sanjana et al., 2014 | Discontinued, alternative is Pooled Library #1000000052 |
| mGeCKOb | Sanjana et al., 2014 | Discontinued, alternative is Pooled Library #1000000052 |
| Software and Algorithms | | |
| FlowJo software 9.9.6 | FlowJo | https://www.flowjo.com |
| Cutadapt | Martin, 2011 | https://cutadapt.readthedocs.io/en/stable/ |
| Bowtie 1.1.2 | Langmead et al., 2009 | http://bowtie-bio.sourceforge.net |

(*Continued on next page*)

*Continued*

| REAGENT or RESOURCE | SOURCE | IDENTIFIER |
|---|---|---|
| DAVID | Huang et al., 2009 | https://david.ncifcrf.gov |
| Cell Ranger 1.3 | 10x Genomics (Zheng et al., 2017b) | https://www.10xgenomics.com/solutions/single-cell/ |
| Seurat | Butler et al., 2018 | https://satijalab.org/seurat/ |
| Scran R package | Lun et al., 2016 | https://www.r-project.org |
| Rtsne R package | van der Maaten, 2014; van der Maaten and Hinton, 2008 | https://www.r-project.org |
| Edge R package | Robinson et al., 2010 | https://www.r-project.org |
| RIGER | Luo et al., 2008 | https://software.broadinstitute.org/GENE-E/extensions.html |
| MAGeCK | Li et al., 2014 | https://sourceforge.net/p/mageck/wiki/Home/ |
| Kallisto | Bray et al., 2016 | https://pachterlab.github.io/kallisto/ |
| Sleuth | Pimentel et al., 2017 | https://pachterlab.github.io/sleuth/ |
| GSEA | Subramanian et al., 2005 | http://software.broadinstitute.org/gsea/index.jsp |
| PSCAN | Zambelli et al., 2009 | http://159.149.160.88/pscan/ |

## LEAD CONTACT AND MATERIALS AVAILABILITY

Further information and requests for resources and reagents should be directed to and will be fulfilled by the Lead Contact, Sidi Chen (sidi.chen@yale.edu). A list of critical reagents (key resources) is included in the Key Resources Table. Relevant plasmids are deposited to Addgene and available to the academic community. For additional materials, please email the lead contact for requests. Some material may require requests to collaborators and/or agreements with various entities. Requests are reviewed by Yale University regarding intellectual property or confidentiality obligations. Material that can be shared will be released via a Material Transfer Agreement.

## EXPERIMENTAL MODEL AND SUBJECT DETAILS

### Mice

All animal work was approved by IACUC and performed with approved protocols (Chen-2015-20068; Chen-2018-20068). Mice, both sexes, between the ages of 6-12 weeks of age were used for the study. OT-I TCR transgenic mice (OT-I mice) were described by (Hogquist et al., 1994). Constitutive Cas9-2A-EGFP mice (Cas9 mice) were described by (Chu et al., 2016; Platt et al., 2014). *Rag1*$^{-/-}$ were described by (Mombaerts et al., 1992). OT-I;Cas9 mice were generated by breeding OT-I and Cas9 mice and genotyped according to Jackson Lab protocol. Naive CD8 T cells were isolated from OT-I mice, Cas9 mice, and OT-I;Cas9 mice using Miltenyi bead-based kits. Tumor-transplantation studies were conducted in *Rag1*$^{-/-}$ mice. All animals were housed in standard individually ventilated, pathogen-free conditions, with 12h:12h or 13h:11h light cycle, room temperature (21-23°C) and 40%–60% relative humidity. When a cohort of animals were receiving multiple treatments, animals were randomized by 1) randomly assign animals to different groups using littermates, 2) random mixing of females prior to treatment, maximizing the evenness or representation of mice from different cages in each group, and/or 3) random assignment of mice to each group, in order to minimize the effect of gender, litter, small difference in age, cage, housing position, where applicable. Average tumor sizes were consistent between treatment groups to account for selection bias.

## METHOD DETAILS

### Generation of a T cell CRISPR vector

A lentiviral T cell CRISPR vector, lenti-pLKO-U6-sgRNA(BsmBI)-EFS-Thy1.1CO-spA, was generated by codon-optimizing and subcloning Thy1.1 and sgRNA expression cassette into a lentiviral vector via Gibson assembly. Vector expresses an sgRNA with a non-targeting spacer.

### Genome-scale mouse T cell CRISPR library cloning

Two sub-libraries (mGeCKOa and mGeCKOb) from (Sanjana et al., 2014) were sub-cloned in equal molar ratios by Gibson assembly into the T cell CRISPR vector to generate the genome-scale mouse T cell CRISPR library (MKO). The resulting library consisted of

129,209 sgRNAs including 1,000 non-targeting controls (NTCs) and 128,209 unique sgRNAs targeting every gene in the genome. An estimated library coverage of > 50x (~7 × $10^6$ total colonies) was achieved by electroporation. The library was subsequently sequence-verified by Illumina sequencing.

### Viral library production

The MKO library plasmid was transfected into low-passage HEK293FT cells at 80% confluency in 15cm tissue culture plates. Viral supernatant was collected at 48h and 72h post-transfection, filtered via a 0.45 μm filtration unit (Fisher/VWR), and concentrated using AmiconUltra 100kD ultracentrifugation units (Millipore). The concentrated supernatant was subsequently aliquoted and stored in −80°C until use. Virus for empty vector was produced in a similar manner.

### T cell isolation and culture

Spleens and mesenteric lymph nodes (mLNs) were isolated from indicated mouse strains and placed in ice-cold 2% FBS [FBS (Sigma) + PBS (GIBCO)]. Organs were prepared by mashing organs through a 100 μm filter. Lymphocytes were suspended in 2% FBS. RBCs were lysed with ACK Lysis Buffer (Lonza), incubated for 2 mins at room temperature, and washed with 2% FBS. Lymphocytes were filtered through a 40 μm filter and resuspended with MACS Buffer (PBS + 0.5% BSA + 2 μM EDTA). Naive CD8 T cells were isolated using naive mouse CD8 T cell isolation kit from Miltenyi. Naive CD8 T cells were resuspended with cRPMI (RPMI-1640 + 10% FBS + 2mM L-Glutamine + 100U Pen/Strep (Fisher) + 49nM β-mercaptoethanol (Sigma)) to a final concentration of 1 × $10^6$ cells/ml. Medium for *in vivo* experiments was supplemented with 2ng/ml IL-2 + 2.5ng/ml IL-7 + 50ng/ml IL-15 + 1 μg/ml anti-CD28. Medium for *in vitro* experiments was supplemented with 2ng/ml IL-2 + 2ng/ml IL-12p70 + 1 μg/ml anti-CD28. Cells were cultured on plates pretreated with 5 μg/ml anti-CD3. Cytokines and antibodies mentioned above were purchased from BioLegend.

### T cell transduction, virus titration

T cells were infected in culture immediately after isolation by directly adding concentrated virus into the media. Cells were cultured for 3 days after viral transduction to provide sufficient time for sgRNA expression. T cells were stained for Thy1.1 expression to determine viral transduction efficiency and analyzed on FACS. Viral titer was determined for each batch by the number of Thy1.1$^+$ T cells normalized to total T cells divided by the volume of virus used. At least 3 doses of viruses with experimental duplicates were used for determining viral titer.

### Antibody and Flow Cytometry

Infectivity of CD8 T cells was assessed via surface staining with anti-CD3ε APC, anti-CD8α FITC, and anti-Thy1.1 PE. Biolegend antibodies used in experiments anti-CD3ε PE/Cy7, anti-CD8α APC, anti-CD16/32, anti-CD27 PE, anti-CD44 PE, anti-CD45 PerCP/Cy5.5, anti-CD62L PE, anti-CD69 PE, anti-CD107a PE, anti-CD279 PE, anti-IFNγ APC, anti-Granzyme B PE, anti-Lag3 PE, anti-SIINFEKL:H-2K$^b$ PE, anti-Thy1.1 PE, and anti-Tim3 PE. Anti-human/mouse DHX37/Dhx37 purchased from Novus Biologicals and anti-NF-κB p65 purchased from Invitrogen were used for immunoblotting. Anti-human DHX37 and anti-human PDCD11 purchased from Bethyl Laboratory was used for immunoprecipitation. Anti-β-actin purchased from Invitrogen and anti-GAPDH purchased from Santa Cruz Biotechnology was used for loading control. For surface stains, cells were stained on ice for 30 mins. Samples were collected on a BD FACSAria cell sorter with 3 lasers, and analyzed using FlowJo software 9.9.6 (Treestar, Ashland, OR) on a MAC workstation.

### Library-scale viral transduction of T cells

T cells were isolated and cultured as described previously. Similar to previous studies (Chen et al., 2014; Zhou et al., 2014), for each infection replicate, a total of > 1 × $10^8$ Cas9 or naive OT-I; Cas9 CD8 T cells were transduced with concentrated lentivirus containing the MKO library described above, to achieve an initial library coverage of > 700x. Transduction with the virus containing the empty vector was performed in parallel with a total of > 1 × $10^7$ naive CD8 T cells. Multiple computational strategies were used to generate quantitative ranked list of genes and to distinguish mis-associations or false-positives from potential true hits with strong selection, including usage of independent infection replicates, different mice, independent screens, different TCRs, and independent sgRNAs (later in methods). In each experiment, 3 infection replicates were applied for generation of T cell library unless otherwise noted.

### Adoptive transfer of viral library infected T cells

At day 0 of the culture, naive CD8 T cells were infected with the lentiviral MKO library and incubated at 37°C for 3 days. On day 3 of culture, T cells were collected, washed with ice-cold PBS, and resuspended to a final concentration of 5 × $10^7$ cells/ml. 1 × $10^7$ cells were injected intravenously into each mouse. All adoptive cell transfer experiments in this study were done without lymphodepletion. On 7-day post-transfer, mice were euthanized, and relevant organs were isolated.

### Generation of a model antigen expression vector

A lentiviral mCherry-OVA (mCh-OVA) vector, lenti-pLKO-U6-sg(BsmBI)-EFS-mCherry-2A-OVA, was generated by subcloning OVA into a mCherry lentiviral vector via Gibson assembly.

### Generation of mCherry-OVA cell line

E0771 murine breast cancer cells were transduced with mCh-OVA-expressing lentivirus. After 3 days post-transduction, transduced E0771 cells were cultured individually in 96-well plate by resuspending cells to 10 cells/ml and culturing 100 μL of cell suspension in each well. 2 weeks later, clonal $mCh^+$ E0771 clones were identified by fluorescence light microscopy. $mCh^+$ E0771 clones were stained with established anti-mouse SIINFEKL: H-$2K^b$ antibody (Porgador et al., 1997) to determine OVA expression. Different E0771-mCh-OVA clones were selected based on OVA expression. Clone 3 was chosen for *in vivo* experiments because of its low, uniform expression of OVA to select for genes with stronger phenotypes.

### Tumor transplantation and tissue processing

$5 \times 10^6$ E0771-mCh-OVA cells were either injected either subcutaneously or into the mammary fat pad of *Rag1*$^{-/-}$ mice. 10 days post-transplantation, viral library infected T cells, prepared as previously described, were intravenously injected in tumor-bearing *Rag1*$^{-/-}$ mice. After 7 days, draining lymph nodes, non-draining lymph nodes, spleens, lungs, and tumors were isolated. Samples were prepared for DNA extraction or FACS analysis. Spleens and lymph nodes were prepared as previously described. Tumors were broken down into smaller fragments, about the size of lentils. Tumors were then dissociated with 1 μg/ml Collagenase IV for 30 minutes using GentleMacs Octo Dissociator from Miltenyi, and cell suspensions were passed through 100 μm filter twice before staining.

### Antigen specificity testing for OT-I T cells

Naive CD8 T cells were isolated from OT-I; Cas9 mice using Naive mouse CD8 T cell kit from Miltenyi. Cells were cultured for 3 days in the presence of plate bound anti-CD3 (5ug/ml), soluble anti-CD28 (1ug/ml), recombinant mouse IL-2 (2ng/ml), recombinant mouse IL-7 (5ng/ml), and recombinant mouse IL-15 (50ng/ml). Cells were analyzed for their activation status through flow cytometric analysis of anti-CD44 PE and anti-CD69 PE. $5 \times 10^6$ cells were adoptively transferred into Rag1$^{-/-}$ mice. After 7 days, these mice were sacrificed, spleens were harvested, and prepared similarly to methods described previously. CD8 T cells were purified using mouse CD8 T cell kit from Miltenyi. Cells were then resuspended to a final concentration of $1 \times 10^6$ cells/ml in cRPMI supplemented with IL-2, IL-2, monensin, and anti-CD107a. Cells were then cocultured with either E0771 cells or E0771-mChOVA cells for 2 hours. After 2 hours, samples were stained with anti-CD3 PE/Cy7 and anti-CD8 APC, and analyzed via flow cytometry.

### Degranulation screen and validation

Experiments were first optimized by pulsing E0771 cells with varying concentrations of SIINFEKL peptide for 4 hours at 37°C, and subsequently stained with the anti-mouse SIINFEKL: H-$2K^b$ antibody and analyzed on flow cytometry. The dose of 1ng/ml was chosen as it represents the maximum concentration tested without being detected by anti-SIINFEKL: H-$2K^b$. Naive OT-I; Cas9 CD8 T cells were isolated and transduced with MKO lentiviral library as previously described. Infected OT-I; Cas9 CD8 T cells were incubated on plates pretreated with 5 μg/ml anti-CD3ε in cRPMI supplemented with 2ng/ml IL-2 + 2ng/ml IL-12p70 + 1 μg/ml anti-CD28 for 6 days. 12 hours before assay, infected OT-I; Cas9 CD8 T cells were incubated on untreated plates in the presence of 2ng/ml IL-2 + 2ng/ml IL-12p70 to rest cells. On day 6, 12 hours before assay, $1 \times 10^7$ E0771 cells were also plated on 10cm plate in D10 media (DMEM + 10% FBS + 100U Pen/Strep). The following day, E0771 cells were incubated with warm D10 media supplemented with either 0 or 1ng/ml SIINFEKL peptide for 4 hours. Meanwhile, infected OT-I; Cas9 CD8 T cells were resuspended to a final concentration $1 \times 10^6$ cells/ml with cRPMI + 2nM monensin + anti-CD107a PE antibody (1:400), and added to E0771 cells at a T cell: seeding cancer cell ratio = 1:1. Cells were co-incubated at 37°C for 2 hours. Cells were then stained with anti-CD8 APC for 30 minutes on ice, and cells were sorted via BD FACSAria. $1 \times 10^7$ T cells were analyzed, and the top 5% $CD107a^+$ cells were sorted, and subjected to genomic DNA extraction, CRISPR library readout, and screen data analysis (described below). A total of three biological replicates were performed. In Dhx37 single gene perturbation degranulation assay, both T cell and E0771 cells were scaled down accordingly, while maintaining T cell: seeding cancer cell ratio = 1:1. Briefly, cells are infected and cultured at 37°C for 7 days. On day 6, T cells are rested overnight and E0771 cells are plated in 24-well plate at $5 \times 10^5$ cells/ml/well. E0771 cells are then incubated with media, 1ng/ml SIINFEKL or 10ng/ml SIINFEKL for 4 hours in D10 media. $5 \times 10^5$ OT-I; Cas9 CD8 T cells were added to the pulsed E0771 cells. During co-culture, IL-2, IL-12, anti-CD107a-PE (1:400), and monensin was added. After 2 hours of incubation, cells were isolated, stained, and analyzed by flow cytometry.

### Genomic DNA extraction

For gDNA extraction, three methods were used. Method 1: for samples with a total number of less than or equal to $1 \times 10^5$ cells, 100 μL of QuickExtract solution (Epicenter) was directly added to cells and incubated at 65°C for 30 to 60 minutes until the cell pellets were completely dissolved followed by a 5 minute incubation at 95°C to denature proteins found in QuickExtract. Method 2: for cellular samples with a total number of $1 \times 10^5$ to $2 \times 10^6$ cells, or tissue samples from mouse lymph nodes, samples were subjected to QIAamp Fast DNA Tissue Kit (QIAGEN) following the manufacturer's protocol. Method 3: for cellular samples with a total number greater than $2 \times 10^6$ cells, or tissue samples from mouse organs or tumor samples, a custom Puregene protocol was used. Briefly, 50-200 mg of frozen ground tissue were resuspended in 6 mL of Lysis Buffer (50 mM Tris, 50 mM EDTA, 1% SDS, pH 8) in a 15 mL conical tube, and 30 μL of 20 mg/ml Proteinase K (QIAGEN) were added to the tissue/cell sample and incubated at 55°C overnight. The next day, 30 μL of 10 mg/ml RNase A (QIAGEN) was added to the lysed sample, which was then inverted 25 times and incubated

at 37°C for 30 minutes. Samples were cooled on ice before addition of 2 mL of pre-chilled 7.5M ammonium acetate (Sigma) to precipitate proteins. The samples were vortexed at high speed for 20 s and then centrifuged at ≥ 4,000 x *g* for 10 minutes. Then, a tight pellet was visible in each tube and the supernatant was carefully decanted into a new 15 mL conical tube. Then 6 mL 100% isopropanol was added to the tube, inverted 50 times and centrifuged at ≥ 4,000 x *g* for 10 minutes. Genomic DNA was visible as a small white pellet in each tube. The supernatant was discarded, 6 mL of freshly prepared 70% ethanol was added, the tube was inverted 10 times, and then centrifuged at ≥ 4,000 x *g* for 1 minute. The supernatant was discarded by pouring; the tube was briefly spun, and remaining ethanol was removed using a P200 pipette. After air-drying for 10-30 minutes, the DNA changed appearance from a milky white pellet to slightly translucent. Then, 500 μL of $ddH_2O$ was added, the tube was incubated at 65°C for 1 hour and at room temperature overnight to fully resuspend the DNA. The next day, the gDNA samples were vortexed briefly. The gDNA concentration was measured using a Nanodrop (Thermo Scientific).

### sgRNA library readout by deep sequencing

The sgRNA library readout was performed using a two-steps PCR strategy, where the first PCR includes enough genomic DNA to preserve full library complexity and the second PCR adds appropriate sequencing adapters to the products from the first PCR.

For PCR#1, a region containing sgRNA cassette was amplified using primers specific to the T cell CRISPR vector:

Forward CCCGAGGGGACCCAGAGAG
Reverse CAATTCCCACTCCTTTCAAGAC

PCR was performed using Phusion Flash High Fidelity Master Mix (PF) or DreamTaq Green PCR Master Mix (DT) (ThermoFisher). For reactions using PF, in PCR#1, the thermocycling parameters were: 98°C for 2min, 18-24 cycles of (98°C for 1 s, 62°C for 5 s, 72°C for 30 s), and 72°C for 2 minutes. For reactions using DT, the thermocycling parameters were adjusted according to manufacturer's protocol. In each PCR#1 reaction, we used 3 μg of total gDNA. For each sample, the appropriate number of PCR#1 reactions was used to capture the full representation of the screen. For example, at ~200x coverage of our 129,209 MKO sgRNA library, gDNA from $2.5 \times 10^7$ cells was used. Assuming 6.6 pg of gDNA per cell, ~160 μg of gDNA was used per sample, in approximately 50 PCR#1 reactions (with ~3 μg of gDNA per reaction).

PCR#1 products for each biological sample were pooled and used for amplification with barcoded second PCR primers (Supplementary Tables). For each sample, we performed at least 4 PCR#2 reactions using 2 μL of the pooled PCR#1 product per PCR#2 reaction. Second PCR products were pooled and then normalized for each biological sample before combining uniquely barcoded separate biological samples. The pooled product was then gel purified from a 2% E-gel EX (Life Technologies) using the QiaQuick kit (QIAGEN). The purified pooled library was then quantified with a gel-based method using the Low-Range Quantitative Ladder Life Technologies, dsDNA High-Sensitivity Qubit (Life Technologies), BioAnalyzer (Agilent) and/or qPCR. Diluted libraries with 5%–20% PhiX were sequenced with MiSeq, HiSeq 2500 or HiSeq 4000 systems (Illumina).

### T cell adoptive transfer anti-tumor efficacy

sgRNAs targeting individual genes were cloned into the T celal CRISPR vector. Two independent sgRNAs targeting each gene (e.g., *Dhx37*) were used. Virus prep and T cell infection were performed as described above. $5 \times 10^6$ E0771-mCh-OVA cells were injected either subcutaneously or into the intramammary fat pad of *Rag1*$^{-/-}$ mice. 7 days post-transplantation, freshly isolated naive OT-I; Cas9 CD8 T cells were plated on plates pretreated with 5 μg/ml anti-CD3ε in cRPMI supplemented with 2ng/ml IL-2 + 2.5 ng/mL IL-7 + 50 ng/mL IL-15 + 1 μg/ml anti-CD28, infected with these sgRNA-containing lentiviruses (at MOI of ~ = 1) as described above, and cultured for 3 days. 10 days post-transplantation, $5 \times 10^6$ virally infected T cells were intravenously injected in tumor-bearing *Rag1*$^{-/-}$ mice (T cell: initial cancer cell ratio = 1:1). PBS and empty vector infected T cells were used as adoptive transfer controls. Tumor sizes were measured by caliper once to twice per week. 6 weeks after adoptive transfer, tumors were dissected, and samples were subjected to molecular, cellular, histology analysis, or single-cell RNA-seq. For statistical comparison of tumor growth curves, multiple t tests were performed (Benjamini, Krieger and Yekutieli FDR method) on each time point.

### Tumor cell preparation and Tumor Infiltration Lymphocyte Isolation

Tumor bearing mice were euthanized at designated time points, and their tumors were collected and kept in ice cold 2% FBS. Tumors were minced into 1-3 mm size pieces using scalpel and then digested in 1 μg/ml Collagenase IV for 30-60 min using Miltenyi GentleMACS Octo Dissociator. Tumor suspensions were filtered twice through 100μm cell strainer, and again through 40μm cell strainer to remove large bulk. For antigenic retention experiments, $10^8$ cells were stained with 4ml of MACS Buffer and Live/Dead fixable near-IR dead cell stain from Invitrogen for 15 minutes on ice. Samples were washed twice with MACS Buffer. Tumor cell suspensions were filtered twice through 40μm cell strainer before FACS data acquisition.

For tumor infiltration lymphocyte (TIL) isolation, tumor suspensions were carefully layered onto Ficoll-Paque media (GE Healthcare) and centrifuge at 400 g for 30 min to enrich lymphocytes at the bilayer interface. Cells at the interface were carefully collected, and washed twice with 2% FBS, counted, and stained with indicated antibodies for 30 minutes on ice. $CD3^+CD8^+$ TILs were then sorted on BD FACSAria. A total of $3 \times 10^3$ to $2 \times 10^4$ TILs were collected per tumor.

### TIL single cell RNA-seq

TILs sorted from freshly isolated tumors were subjected to single-cell RNA-seq library prep. We followed a protocol by 10x Genomics to perform single cell RNA-seq (scRNA-seq). In brief, Single Cell Master Mix was prepared fresh containing RT reagent mix, RT primer, additive A, and RT enzyme mix. A Single Cell 3′ Chip was placed in a 10x Chip Holder. 50% glycerol solution to each unused well accordingly, TIL solution at ~100 cell / μl was added together with the master mix. The Single Cell 3′ Gel Bead Strip was placed into a 10x Vortex Adaptor and vortex for 30 s. Then, Single Cell 3′ Gel Bead suspension and Partitioning Oil were dispensed into the bottom of the wells in the specified rows. The fully loaded chip was then inserted into Chromium Controller to generate emulsion. The emulsion was then transferred to a 96-well PCR plate for GEM-RT reaction, RT clean up, cDNA amplification, cDNA clean-up, quantification and QC, and subjected to Illumina library construction. In library construction, clean input cDNA was then subjected to fragmentation, end repair & A-tailing. After that, double sided size selection was performed using SPRI Select, followed by adaptor ligation, clean up, and sample indexing PCR, pooling and PCR cleanup, resulting a single-cell RNA-seq library. Enzymatic Fragmentation and Size Selection were used to optimize the cDNA amplicon size prior to library construction per manufacturer's protocols. R1 (read 1 primer sequence) are added to the molecules during GEM incubation. P5, P7, a sample index and R2 (read 2 primer sequence) are added during library construction via end repair, A-tailing, adaptor ligation and PCR. The Single Cell 3′ Protocol produces Illumina-ready sequencing libraries contain the P5 and P7 primers used in Illumina bridge amplification. This final library was then QC'ed and quantified using BioAnalyzer, and loaded on a Hiseq 2500 RapidRun for standard Illumina paired-end sequencing, where Barcode and 10 bp randomer (UMI) is encoded in Read 1, while Read 2 is used to sequence the cDNA fragment. Sample index sequences are incorporated as the i7 index read.

### AAV T cell knockout vector

An adeno-associated virus (AAV) CRISPR T cell knockout vector, pAAV-U6-sgBbsI-EFS-Thy1.1-PolyA, was generated by subcloning Thy1.1 and sgRNA expression cassette into an AAV vector via Gibson Assembly (NEB). Vector expresses an sgRNA with a non-targeting spacer. For individual gene targeting, the AAV knockout vector was digested with BbsI. Oligonuleotides encoding specific sgRNAs were ligated into the digested AAV knockout vector using T4 ligase (NEB).

### AAV virus production

Various AAV knockout plasmids used in this study as described in the figures and results were subjected to AAV production and chemical purification. Briefly, HEK293FT cells (ThermoFisher) were transiently transfected with transfer (AAV-plasmids), serotype (AAV9 or AAV6) and packaging (pDF6) plasmids using polyethyleneimine (PEI). Approximately 72 h post-transfection, cells were dislodged and transferred to a conical tube in sterile PBS. 1/10 volume of pure chloroform was added to the mixture and incubated at 37°C for 1 h. NaCl was added to a final concentration of 1 M. The mixture was subsequently shaken until dissolved and then pelleted at 20,000 gx at 4°C for 15 min. The chloroform layer was discarded while the aqueous layer was transferred to another tube. PEG8000 was added to 10% (w/v) and shaken until dissolved. The mixture was incubated at 4°C for 1 h and spun at 20,000 gx at 4°C for 15 min. After the supernatant was discarded, the pellet was resuspended in DPBS + $MgCl_2$, treated with benzonase (Sigma), and then incubated at 37°C for 30 min. Chloroform (1:1 volume) was then added, shaken and spun down at 12,000 g at 4°C for 15 min. The aqueous layer was isolated and passed through a 100-kDa MWCO (Millipore). The concentrated solution was washed with PBS and the filtration process was repeated. Virus was titered by qPCR using custom Taqman assays (ThermoFisher).

### Immunological characterization

For immunological characterization, naive OT-I; Cas9 CD8 T cells were isolated and prepared similarly to methods described previously. At the start of culture, AAV-Vector or AAV-Dhx37 was added to the start of culture. Cells were incubated for 6 days. On the $6^{th}$ day, cells were rested overnight in the presence of IL-2 (2ng/ml) and IL-7 (5ng/ml) for 12 hours. The next day cells were subjected to both functional (degranulation and IFNγ production) and phenotypic analysis (surface and endosomal staining).

### Determining gene editing efficiency

Cutting efficiency was analyzed from cells cultured for 5 days in the presence of AAV. DNA from cells was extracted by incubating cells with Epicenter QuickExtract for 65°C for 30 minutes, and subsequently incubated at 98°C for 5 minutes. gDNA from samples was amplified by PCR. Purified PCR product was subjected to both T7 endonuclease surveyor (NEB) and Nextera sequencing according to Illumina protocol. A list of oligos for T cell gene editing and determination of efficiency can be found at Table S7.

### Western Blot of Dhx37 knockout murine T cells

Pellets from $5 \times 10^6$ cells AAV-Vector or AAV-Dhx37 treated OT-I; Cas9 CD8 T cells were weighed. 10x volume of Invitrogen Lysis Buffer was added to cell pellets. Samples were incubated on ice for at least 10 minutes and then subjected to BCA analysis. 20ug of protein was used for western blot analysis. Dhx37 was analyzed using antibody purchased from Novus Biologicals. Beta-actin was analyzed using antibody purchased from Invitrogen.

### Co-immunoprecipitation

Human PB $CD4^+$, $CD8^+$ T cells, as well as patient TILs were analyzed for DHX37 protein expression by western blot with a rabbit polyclonal antibody (Novus, NBP2-13922). For immunoprecipitation studies, $10^8$ human CD8 T cells were isolated and wash twice with ice cold PBS. The cell pellet was subsequently weighed and 10x volume of Invitrogen Lysis Buffer supplemented with protease inhibitor cocktail (Roche) was added to cell pellets. Samples were incubated on ice for at least 10 minutes and then subjected to BCA analysis. 1-2mg of protein was used for immunoprecipitation studies, 10ug of anti-human DHX37 (Bethyl Laboratories), anti-human PDDC11 (Bethyl Laboratories), or IgG isotype control (Cell Signaling), and volume was resuspended to a final concentration of 400ul Invitrogen Lysis Buffer. Samples were tumbled overnight at 4°C for at least 12 hours. Immunocomplexes were pulled down using Protein A dynabeads from Invitrogen for 6 hours at 4°C. Afterward, beads were washed 3 times with ice cold PBS and resuspended with 50ul of NuPAGE LDS sample buffer with β-ME. Samples were heated at 70°C for 10 minutes. Beads were removed by magnet and eluent transferred to fresh tube. Samples were then heated at 95°C for 3 minutes and placed on ice for 1 minute before immunoblotting. For proteins > 200kDa, 3∼8%Tris-Acetate gels were used for gel electrophoresis. For smaller proteins, 4∼20% Tris-Glycine gels were used. Proteins were then transferred to 0.45 μm PVDF membrane overnight. Membranes were blocked with 5% BSA, stained with primary antibody overnight at 4°C, and stained with VeriBlot for IP secondary antibody (Abcam) for 1 hour at room temperature. Proteins were detected using Pierce ECL substrate.

### qPCR and bulk mRNA-seq

$4 \times 10^6$ cells/sample were washed twice with ice cold PBS. Cells were then treated with TRIzol for 5 minutes at RT. RNA was purified via PureLink RNA mini kit from Invitrogen. cDNA for qPCR was generated using SuperScript Reverse Transcriptase IV users' protocol. In brief, at least 500ng of RNA was used per reaction. Random hexamers were used for cDNA generation. Afterward, cDNA was subjected to qPCR using TaqMan Real-Time PCR Master Mixes. The following probes and their sequences are provided: *Actb* (Mm02619580_g1), *Dhx37* (Mm01202964_g1), *Gapdh* (Mm99999915_g1), *Gzmc* (Mm01313651_m1), *Gzmd* (Mm01722569_g1), *Havcr2* (Mm00454540_m1), *Il6ra* (Mm00439653_m1), *Serpinb9b* (Mm00488405_m1), *Sytl2* (Mm01317927_m1). Samples were processed using Applied Bioscience StepOnePlus Real Time machine and relative mRNA expression was normalized to *Actb* or *Gapdh* controls. Quadruplicate total RNA samples from each group were subjected to mRNA-seq library prep. TruSeq strand-specific kit (Illumina) was used for mRNA-seq library preparation and sequenced using Illumina HiSeq 4000 or Novaseq platforms.

### Endosomal staining

Endosomal staining was performed using BD Cytofix/Cytoperm staining kit and protocol. Prior to endosomal staining, cells were stained with surface markers for 30 minutes on ice. Afterward, cells were fixed with BD Cytofix buffer for 10 minutes on ice. Cells were washed with Cytoperm/Wash Buffer. Cells were then subjected to FcBlock using anti-CD16/32 (1:250) in Cytoperm/Wash Buffer. Samples were subsequently stained with endosomal stain for 30 minutes on ice, washed twice with Cytoperm/Wash Buffer, and finally resuspended in MACS Buffer prior to FACS analysis.

### De novo IFNγ production

AAV-treated OT-I;Cas9 CD8 T cells were incubated for 6 days to allow for sufficient cutting and protein knock down. On day 6, cells were rested for at least 12 hours in cRPMI supplemented with IL-2 (2ng/ml) and IL-7 (5ng/ml). On day of experiment, 96-well plates were coated with PBS or 1ug/ml anti-CD3 for 1 hour at 37°C. (It is important to note that the outside wells were not used in the assay to account for potential edge effects. To avoid this issue, these wells were filled with PBS.) Wells were washed twice with cRPMI. Cells were resuspended to a final concentration of $10^6$ cells/ml of cRPMI supplemented with IL-2, IL-12, anti-CD28, and Brefeldin A. 100ul of cell suspension was added to each well and incubated for 4 hours at 37°C. Cells were then stained for anti-CD3 PE/Cy7 and anti-CD8 FITC. Cells were then fixed with BD Cytofix/Cytoperm kit as mentioned above and stained intracellularly with anti-IFNγ APC. Samples were analyzed via FACS.

### Co-culture killing

E0771 cells or E0771-mCh-OVA cells were infected with lentivirus bearing Luciferase transgene. Luciferase-positive cells were selected under hygromycin selection. Luciferase-positive cells were plated at a 1:1 ratio with AAV-treated OT-I;Cas9 CD8 T cells at a density of $5 \times 10^5$ cells/ml in cRPMI supplemented with IL-2 and IL-12. For controls E0771-luciferase or E0771-mCh-OVA-luciferase cells were plated in the absence of T cells. After 24 hours, 150ug/ml luciferin was added to each well. Luciferase activity was measured using GE Typhoon 9500. Samples were normalized to E0771-luciferase or E0771-mCh-OVA-luciferase controls.

### Human T cell culture and manipulation

Human CD8 T cells were purified from human PBMCs using Human Naive CD8 T cell kit. Human CD8 T cells were cultured at a concentration of $1\text{-}2 \times 10^6$ cells/ml in X-VIVO 15 media supplemented with 5% Human AB serum + IL-2 (100U/ml). Every 14 days, cells were stimulated with anti-CD3/CD28 dynabeads for 48 hours and removed using magnet.

### DHX37 western blot in human T cells

Human PB $CD4^+$, $CD8^+$ T cells, as well as patient TILs were analyzed for DHX37 protein expression by western blot with a rabbit polyclonal antibody (Novus, NBP2-13922).

### GFP-DHX37 tagging

The lentiviral DHX37 overexpression construct was further engineered by Gibson Assembly to insert either an N-terminal or C-terminal EGFP fusion. GGSG linker was inserted between DHX37 and EGFP to prevent potential steric hinderance. Plasmids were used to transfect or transduce cells to overexpress DHX37 protein.

### Immunofluorescence and microscopy

Cells were fixed by 4% PFA for 5 minutes, washed with 0.1% Triton PBS, and stained. Primary antibodies used: chicken anti-GFP (1:500, Abcam ab290), rabbit anti-nucleolin (1:500, Abcam ab22758), and rabbit anti-Dhx37 (1:200, NBP2-13922). Fluorescent images were captured on a Leica inverted microscope.

### Gene editing in human CD8 T cells

Human CD8 T cells were treated according to methods recently developed in the lab (Dai et al., 2019 Mar;). Briefly, 2-3 × $10^6$ cells were washed two times with ice cold PBS. Cells were then resuspended with 100ul of Buffer R from Neon Electroporation Kit.

For Cas9 RNP based gene editing, T cells were prepared at a density of 2 × $10^5$ cells per 10 μL tip reaction in electroporation Buffer R (Neon Transfection System Kits). RNPs were produced by complexing a two-component gRNA to Cas9. In brief, Cas9 sgRNA was designed to target *DHX37* (sg4-TCTTTAAGCCTCCACCGGAG) using Benchling. Cas9 crRNAs and tracrRNAs were chemically synthesized (Dharmacon or IDT), and suspended in nuclease-free IDTE buffer at a concentration of 160 μM. The crRNA and tracrRNA were mixed at 1:1 ratio and annealed as a guide RNA in Nuclease-Free IDTE buffer at 95°C for 5 min and 37°C for 10 min. RNPs were formed by the addition of SpCas9 nuclease (Dharmacon, IDT) with the 80 μM gRNA (1:2 Cas9 to sgRNA molar ratio) at benchtop for 15 min. RNPs were electroporated immediately after complexing at program 24 (1,600V, 10ms and three pulses). After electroporation, the cells were transferred into 1mL of pre-warmed X-VIVO media (without antibiotics) immediately.

For Cas9 mRNA T cell electroporation, Cas9 mRNA T cell electroporation was similar with Cas9 RNP T cell electroporation. After T cells activation, T cells were mixed with 1 μg Cas9 mRNA (TriLink) and 1 μL annealed DHX37 sg4 (80 μM) per 10 μL tip reaction in electroporation Buffer R (Neon Transfection System Kits). Electric shocked were performed at program 24 (1,600V, 10ms and three pulses). After electroporation, the cells were transferred into 1mL of pre-warmed X-VIVO media (without antibiotics) immediately.

For Cpf1 gene editing, 5ug of Cpf1 mRNA and 5ug of crDHX37 was added to cell suspension. Cell mixture was pipetted up and down several times. The mRNA/crRNA complex were electroporated into human CD8 T cells using 3 pulses of 1600V for a duration of 10ms each pulse. After 5 days in culture, genomic DNA isolated per protocols established above. Cutting efficiency was determined by T7E1 surveyor and Nextera.

## QUANTIFICATION AND STATISTICAL ANALYSIS

### Statistics summary

Statistical analyses and software used are described in this section in detail. All of the statistical details of experiments can be found in the figures, figure legends, results, supplemental tables, and/or Mendeley Data (see also: DATA AND CODE AVAILABILITY), including the statistical tests used, exact value of n, what n represents (e.g., number of animals, number of experimental replicates), definition of center, and dispersion and precision measures (e.g., mean and SEM).

### Demultiplexing and read preprocessing

Raw single-end fastq read files were filtered and demultiplexed using Cutadapt (Martin, 2011). To remove extra sequences downstream (i.e., 3′ end) of the sgRNA spacer sequences, we used the following settings: cutadapt–discard-untrimmed -a GTTTTAGAGC TAGAAATGGC. As the forward PCR primers used to readout sgRNA representation were designed to have a variety of barcodes to facilitate multiplexed sequencing, we then demultiplexed these filtered reads with the following settings: cutadapt -g file:fbc.fasta–no-trim, where fbc.fasta contained the 12 possible barcode sequences within the forward primers. Finally, to remove extra sequences upstream (i.e., 5′ end) of the sgRNA spacers, we used the following settings: cutadapt–discard-untrimmed –g GTGGAAAGG ACGAAACACCG. Through this procedure, the raw fastq read files could be pared down to the 20bp sgRNA spacer sequences.

### Mapping of spacers and quantitation of sgRNAs

Having extracted the 20 bp sgRNA spacer sequences from each demulitplexed sample, we then mapped the sgRNA spacers to the MKO library (Table S1). To do so, we first generated a bowtie index of either sgRNA library using the bowtie-build command in Bowtie 1.1.2 (Langmead et al., 2009). Using these bowtie indexes, we mapped the filtered fastq read files using the following settings: bowtie -v 1–suppress 4,5,6,7–chunkmbs 2000 –best. Using the resultant mapping output, we quantitated the number of reads that had mapped to each sgRNA within the library. To generate sgRNA representation bar plots, we set a detection threshold of 1 read, and counted the number of unique sgRNAs present in each sample.

### Normalization and summary analysis of sgRNAs

We normalized the number of reads in each sample by converting raw sgRNA counts to reads per million (rpm). The rpm values were then subject to $\log_2$ transformation for certain analyses. To generate correlation heatmaps, we used the *NMF* R package (Gaujoux and Seoighe, 2010) and calculated the Pearson correlations between individual samples using $\log_2$ rpm counts. To calculate the cumulative distribution function for each sample group, we first averaged the normalized sgRNA counts across all samples within a given group. We then used the ecdfplot function in the *latticeExtra* R package to generate empirical cumulative distribution plots.

### Enrichment analysis of sgRNAs

We used three criteria to identify the top candidate genes: 1) if an sgRNA comprised $\geq$ 2% of the total reads in at least one organ sample; 2) if an sgRNA was deemed statistically significantly enriched in $\geq$ 20% of all organ samples using a false-discovery rate (FDR) threshold of 0.5% based on the abundances of all non-targeting controls; or 3) if $\geq$ 2 independent sgRNAs targeting the same gene were each found to be statistically significant at FDR < 0.5% in at least one sample each. For the first and second criteria, individual sgRNA hits were collapsed to genes to facilitate comparisons with the hits from the third criteria. Due to the number of T cells trafficking *in vivo* in mice, depletion screen analysis was not performed. To enhance the statistical power, the infiltration screen data from the orthotopic (fat pad) model and the subcutaneous model were combined for hit identification.

### Heatmap sgRNA library representation

Heatmaps of the top enriched sgRNAs were generated using the *aheatmap* function with default setting (*NMF* R package). Only sgRNAs with a $\log_2$ rpm $\geq$ 1 were included for visualization in the heatmaps.

### Overlap and significance of enriched sgRNAs

To generate Venn diagrams of overlapping enriched sgRNAs or genes, we considered all sgRNAs that were found to be significantly across different statistical calling algorithms, different T cells, or different experiments.

### RIGER and MAGeCK analyses

RNAi Gene Enrichment Ranking (RIGER) (Luo et al., 2008) and the Model-based Analysis of Genome-wide CRISPR/Cas9 Knockout (MAGeCK) (Li et al., 2014) algorithms was used as independent methods to quantify enrichment of candidate genes for both the infiltration and survival screens.

For RIGER analysis, read count tables were used to calculate log fold changes for tumor versus cell samples in order to score and rank sgRNAs, with ties in rank broken by random order. This data was then used as input to a Java-based implementation of RIGER (https://github.com/broadinstitute/rigerj) in order to generate p values and gene rankings based on consistent enrichment across multiple sgRNAs for identification of candidate genes (Shalem et al., 2014). Both the second highest-ranking sgRNA and the weighted sum scoring methods were used for computation of gene rankings.

For MAGeCK analysis, read count tables were used as inputs to a command-line-based tool (https://sourceforge.net/p/mageck/wiki/Home/) with the treatment group defined as the tumor samples and the control group defined as the cell pellet samples, with a list of non-targeting control sgRNAs provided for normalization and generation of the null distribution of RRA. Native MAGeCK plotting functions were used for visualization of RRA score and p value distributions and individual sgRNA read counts of selected genes.

### Gene ontology and pathway enrichment analysis

Various gene sets were used for gene ontology and pathway enrichment analysis using DAVID functional annotation analysis (Huang et al., 2009). For sgRNA set, sgRNAs were converted to their target genes and then the resultant genes were used for analysis.

### scRNA-seq data processing

TIL scRNA-seq fastq data was pre-processed using established and custom pipelines. Briefly, raw Illumina data files were subjected to Cell Ranger, which used cellranger mkfastq to wrap Illumina's bcl2fastq to correctly demultiplex Chromium-prepared sequencing samples and to convert barcode and read data to FASTQ files. Then, cellranger count was used to take FASTQ files and performs alignment to mouse genome (mm10), filtering, and UMI counting. Raw sequencing output was first preprocessed by Cell Ranger 1.3 (10x Genomics) (Zheng et al., 2017b) using cellranger mkfastq, count, and aggr (no normalization mode). Cells passed the initial quality control metrics imposed by the Cell Ranger pipeline were further filtered using a variety of criteria (Lun et al., 2016): 1) We excluded all cells with a total library count (i.e., # of UMIs) that was $\geq$ 4 standard deviations below the mean; 2) We excluded all cells with library diversity (i.e., # of detected genes/features) that was $\geq$ 4 standard deviations below the mean; and 3) We excluded all cells in which mitochondrial genes disproportionately comprised the total % of the library ($\geq$4 standard deviations above the mean). After applying these 3 filters, we retained a final set of cells for further analysis. We additionally filtered the 27,998 genes/features using a flat cutoff metric: genes with low variance were excluded. Finally, the data was normalized by library size using the *scran* R package (Lun et al., 2016).

### scRNA-seq analysis

Using the final normalized and processed dataset (described above), we performed differential expression analysis using the *edgeR* R package (Robinson et al., 2010). In brief, *edgeR* first estimates the negative binomial dispersion parameter to model the variance

between cells from the same treatment group. A generalized linear model is then fitted to determine differentially expressed genes between treatment conditions. Multiple hypothesis correction was performed by the Benjamini-Hochberg method. Significantly differentially expressed genes were defined as having a Benjamini-Hochberg adjusted $p < 0.05$, with upregulated genes having a positive log fold change and downregulated genes having a negative log fold change. Volcano plots were generated using *edgeR* output statistics. Gene ontology enrichment analyses on differentially expressed genes were performed using the PANTHER classification system (Mi et al., 2013). The statistical overrepresentation test was used to identify enriched GO (biological process) categories among the differentially expressed genes. Bonferroni multiple hypothesis correction was performed. To generate an overall view of the top differentially expressed genes, we scaled each row of the dataset (i.e., by gene) to obtain z-scores. Heatmaps were generated using the *NMF* R package (Gaujoux and Seoighe, 2010).

### mRNA-seq processing and analysis

Bulk mRNA-seq fastq files were processed by kallisto (Bray et al., 2016), with the settings–rf-stranded –b 100. Differential expression analysis was then performed using Sleuth (Pimentel et al., 2017). Significant differentially expressed genes were defined by a Benjamini-Hochberg adjusted p value < 0.05. Differentially expressed genes were used for DAVID gene ontology analysis (Huang et al., 2009). The full dataset was also used for GSEA (Subramanian et al., 2005). Motif enrichment analysis in the promoters of differentially expressed genes was performed using (Zambelli et al., 2009), using a −450 to +50 bp interval and the TRANSFAC database.

### Epigenetic analysis of Dhx37 in CD8 T cells

Normalized ATAC-seq, H3K4me3, H3K27ac, and H3K27me3 tracks were accessed from GSE111092 (Laumont et al., 2018), through the ctlcon package (https://bitbucket.org/robert_amezquita/ctlcon).

### Analysis of human T cell (sc)RNA-seq data

Human T cell scRNA-seq data from liver cancer patients ((Zheng et al., 2017a), GSE98638) and melanoma patients undergoing immunotherapy ((Sade-Feldman et al., 2018), GSE120575.) For the GSE98638 dataset, cells were classified according to the original definitions: peripheral blood, tissue-resident, tumor-normal junction, and tumor-infiltrating T cells; $CD3^+/CD4^+/CD25^-$ T cells, $CD3^+/CD8^+$ T cells, and $CD3^+/CD4^+/CD25^+$ T cells. For the GSE120575 dataset, the published designations of "exhausted" versus "non-exhausted" were utilized. For both datasets, normalized TPM expression values were utilized for downstream analysis. Differential expression of DHX37 in exhausted versus non-exhausted CD8 T cells was assessed by Mann Whitney test. For analysis of DHX37 expression in bulk RNA-seq data from human T cells, the DICE database was queried (Schmiedel et al., 2018) (https://dice-database.org/).

### Analysis of CTL function in patient survival

We used the TIDE tool with DHX37 as the query gene (Jiang, 2018) (http://tide.dfci.harvard.edu/query/). Breast cancer datasets were evaluated for evidence of T cell dysfunction, stratified by bulk tumor expression levels of DHX37.

### Blinding statement

Investigators were blinded for sequencing data analysis using metadata, but not blinded for tumor engraftment, adoptive transfer, organ and tumor dissection, or flow cytometry.

## DATA AND CODE AVAILABILITY

All data for this study are included in this published article and its supplemental materials. Original/source non-genomics data and relevant statistics for figures in the paper are provided in an excel sheet and are in Mendeley Data (Reserved https://doi.org/10.17632/2ffxmf3d7k.1 at https://doi.org/10.17632/2ffxmf3d7k.1). The genomics data generated during this study are available at public repositories SRA and GEO with Accession numbers. All DNA-level genomic sequencing data are available via NCBI SRA: PRJNA549266. All transcriptomics data are available via GEO (which automatically makes SRA deposit): GSE132960, superseries composed of GSE132926 (bulk RNA) and GSE132959 (scRNA-seq). Custom scripts and additional data related to support the findings of this work will be available to the academic community upon reasonable request to the lead contact.

## ADDITIONAL RESOURCES

Additional resources and related information can be found at Key Resources Table.

Cell

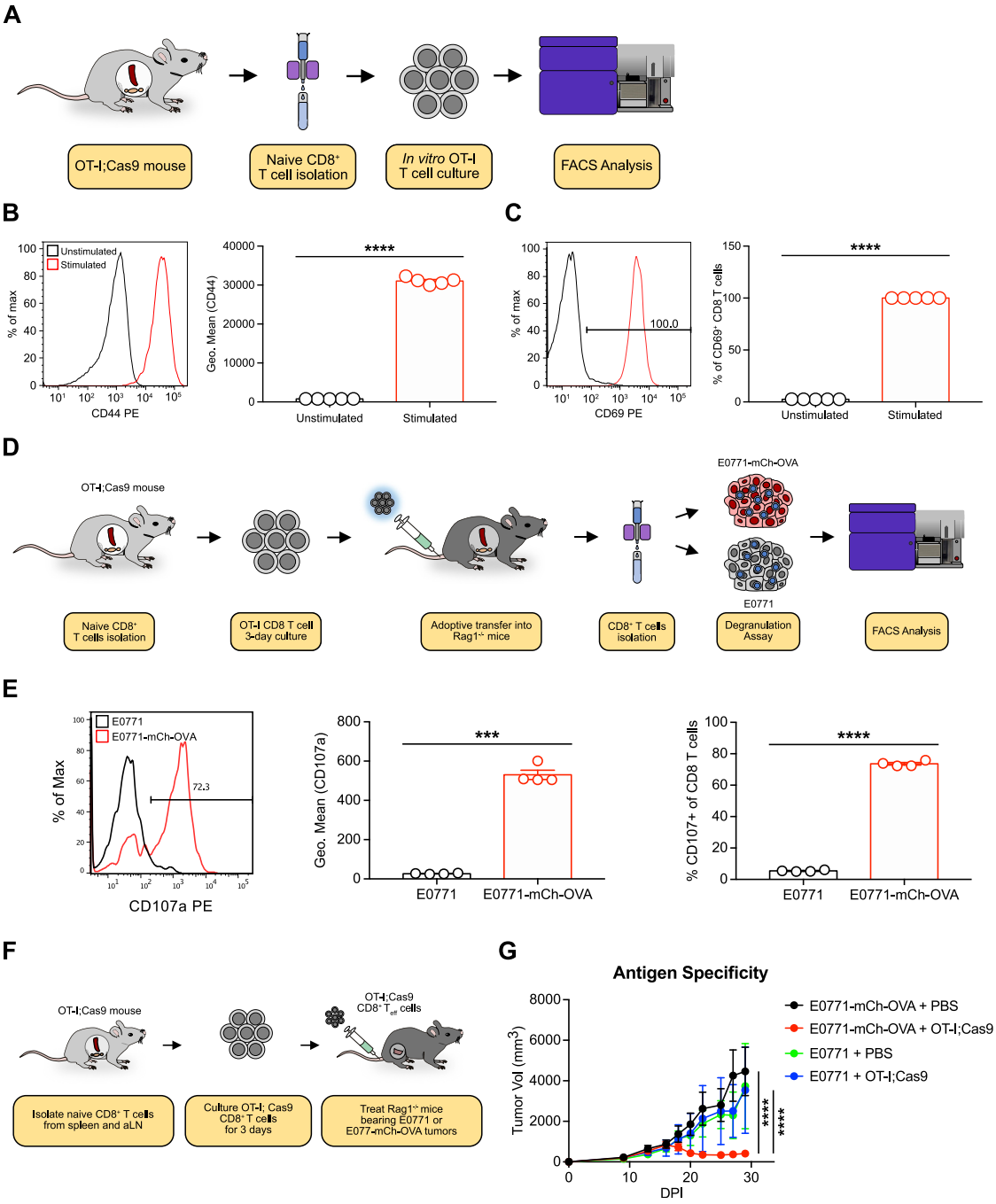


**Figure S1. Testing of Activation and Antigen Specificity of Cas9 and OT-I CD8 T Cells from Transgenic Mice, Related to Figure 1**

(A) Schematic of flow analysis experiment for T cell activation in OT-I;Cas9 CD8 T cells in culture.

(B and C) Flow cytometry analysis of activation markers of T cells, including CD44 (B) and CD69 (C). Left panel in each plot is a representative histogram of stimulated (red) and unstimulated (black) CD8 T cells. Right panel is a bar plot of quantification for each marker. * = $p < 0.05$, ** = $p < 0.01$, *** = $p < 0.001$, by unpaired two-sided t test.

(D) Schematic of flow analysis experiment for antigen-specificity testing in OT-I;Cas9 CD8 T cells in culture.

(E) Flow cytometry analysis of degranulation of T cells using CD107a. Left panel in each plot is a representative histogram of CD8 T cells co-cultured with antigen-expressing cancer cells E0771-mCh-OVA (red) and with parental control cancer cells E0771 (black). Middle panel is a bar plot of quantification for CD107a as geometric mean. Right panel is a bar plot of quantification for CD107a as percent cell positive. * = $p < 0.05$, ** = $p < 0.01$, *** = $p < 0.001$, by unpaired two-sided t test.

(F) Schematic of antigen-specificity testing for OT-I;Cas9 CD8 T cells in a tumor model *in vivo*.

*(legend continued on next page)*

(G) Tumor growth curves of E0771 (parental control line) or E0771-mChOVA (antigen-expressing line) in mice treated with PBS or adoptive transfer of OT-I;Cas9 CD8 T cells. Only the group of E0771-mChOVA tumors receiving adoptive transfer of OT-I;Cas9 CD8 T cells showed significant tumor regression, supporting antigen-specificity of OT-I;Cas9 CD8 T cells against the OVA antigen. * = $p < 0.05$, ** = $p < 0.01$, *** = $p < 0.001$, by two-way ANOVA.

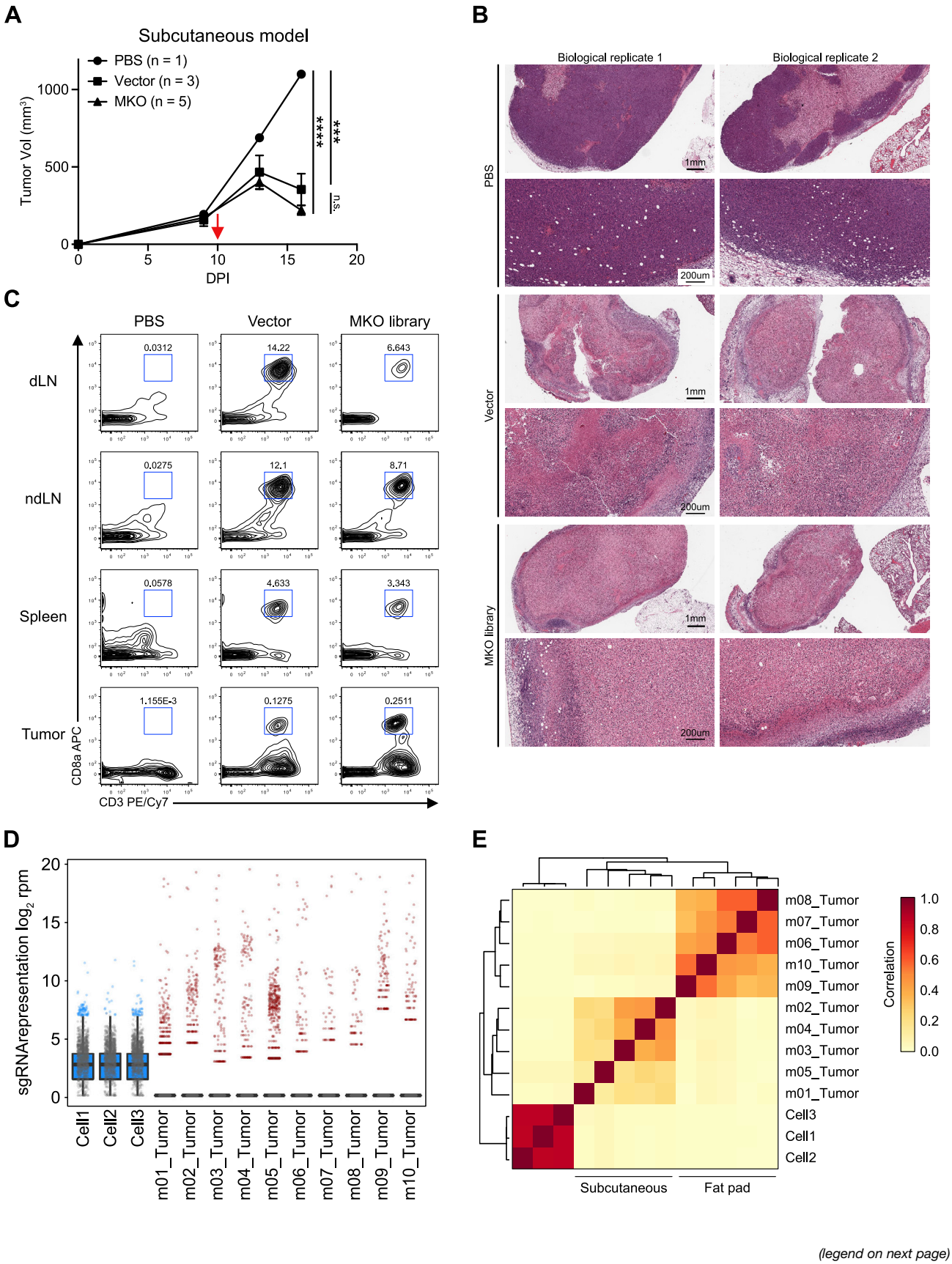


*(legend on next page)*

**Figure S2. Additional Experiments and Analyses for Adoptive Transfer Tumor Infiltration Screen, Related to Figure 1**

(A) Growth curve of subcutaneous tumors from transplanted E0771-mCh-OVA cells in *Rag1*$^{-/-}$ mice following different treatments. PBS control (n = 1), adoptive transfer of OT-I;Cas9 CD8 T cells infected with vector (n = 3), and adoptive transfer of OT-I;Cas9 CD8 T cells infected with MKO (n = 5). Red arrow indicates the time of adoptive transfer of MKO or vector transduced OT-I;Cas9 CD8 T cells. Error bars for certain data points were invisible because the errors were small. Data are shown as mean ± s.e.m.. * = $p < 0.05$, ** = $p < 0.01$, *** = $p < 0.001$, by two-way ANOVA. Note: Detailed statistics related to this figure are provided in an excel table.

(B) Full-slide and high-power histology sections stained by hematoxylin and eosin of tumors derived from E0771 cells expressing OVA antigen in *Rag1*$^{-/-}$ mice after different treatment conditions. Top group: tumors in mice that were injected with PBS. Middle group: tumors in mice after adoptive transfer of vector-treated activated OT-I; Cas9 CD8 T cells. Bottom group: tumors in mice after adoptive transfer of MKO mutagenized activated OT-I; Cas9 CD8 T cells. In PBS group, tumors were devoid of lymphocytes and showed signatures of rapid proliferation and little cell death. In adoptive transfer groups, tumors were infiltrated by lymphocytes and showed signatures of cell death in large areas. Low magnification image scale bar: 1mm; high magnification image scale bar: 200 μm.

(C) Representative FACS plots of adoptively transferred T cells in draining and non-draining LNs (dLN and ndLN, respectively), spleen, lung, and tumor (TILs) from E0771-mCh-OVA tumor-bearing *Rag1*$^{-/-}$ mice. MKO is the genome-scale T cell CRISPR library. Numbers indicate average percentage of total cells. Top row: FACS plots from PBS-treated mice. Middle row: FACS plots from mice treated with vector-infected OT-I;Cas9 CD8 T cells. Bottom row: FACS plots from mice treated with MKO-infected OT-I;Cas9 CD8 T cells.

(D) Box-dot plot of overall sgRNA library representation in all samples, including cellular libraries of infected OT-I;Cas9 CD8 T cells before injection (blue, n = 3), and tumors from multiple mice (red, n = 10 mice, 10 total tumors). sgRNA representation is depicted in terms of $\log_2$ rpm.

(E) Correlation analysis of genome-scale CRISPR perturbation of OT-I;Cas9 CD8 tumor-infiltrating lymphocytes into *Rag1*$^{-/-}$ mice with E0771-mCh-OVA tumors. Heatmap of pairwise Pearson correlations of sgRNA library representation across 3 cell libraries prior to injection, and all samples in the tumor infiltration screen (n = 10 mice, 10 tumors). Correlations were calculated based on $\log_2$ rpm values. E0771-mCh-OVA cells were transplanted subcutaneously for mice 1-5, and into the mammary fat pad for mice 6-10.

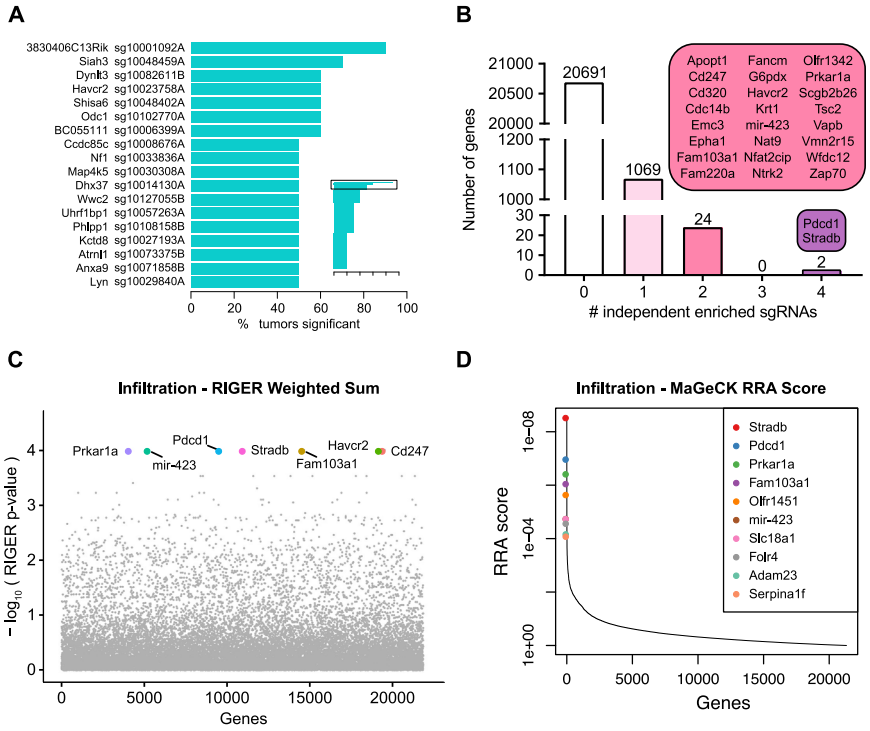


**Figure S3. Additional Analyses for Adoptive Transfer Tumor Infiltration Screen, Related to Figure 1**

(A) Waterfall plot of the top-ranked sgRNAs across all tumors (21 sgRNAs significantly enriched in ≥ 50% of tumors, FDR < 0.5%). Inset, waterfall plot of all sgRNAs that were significantly enriched in ≥ 20% of tumors.

(B) Bar plot of the number of genes with 0-4 independent sgRNAs that were significantly enriched in at least one organ sample (FDR < 0.5%). A total of 26 genes were found to have at least 2 independent sgRNAs enriched. *Pdcd1* and *Stradb* were each found to have 4 independently enriched sgRNAs.

(C) Meta-analysis of infiltration screen using RIGER with Weighted Sum method.

(D) Meta-analysis of infiltration screen using MAGeCK analysis of survival screen, highlighting several top-scoring genes ranked by RRA score.

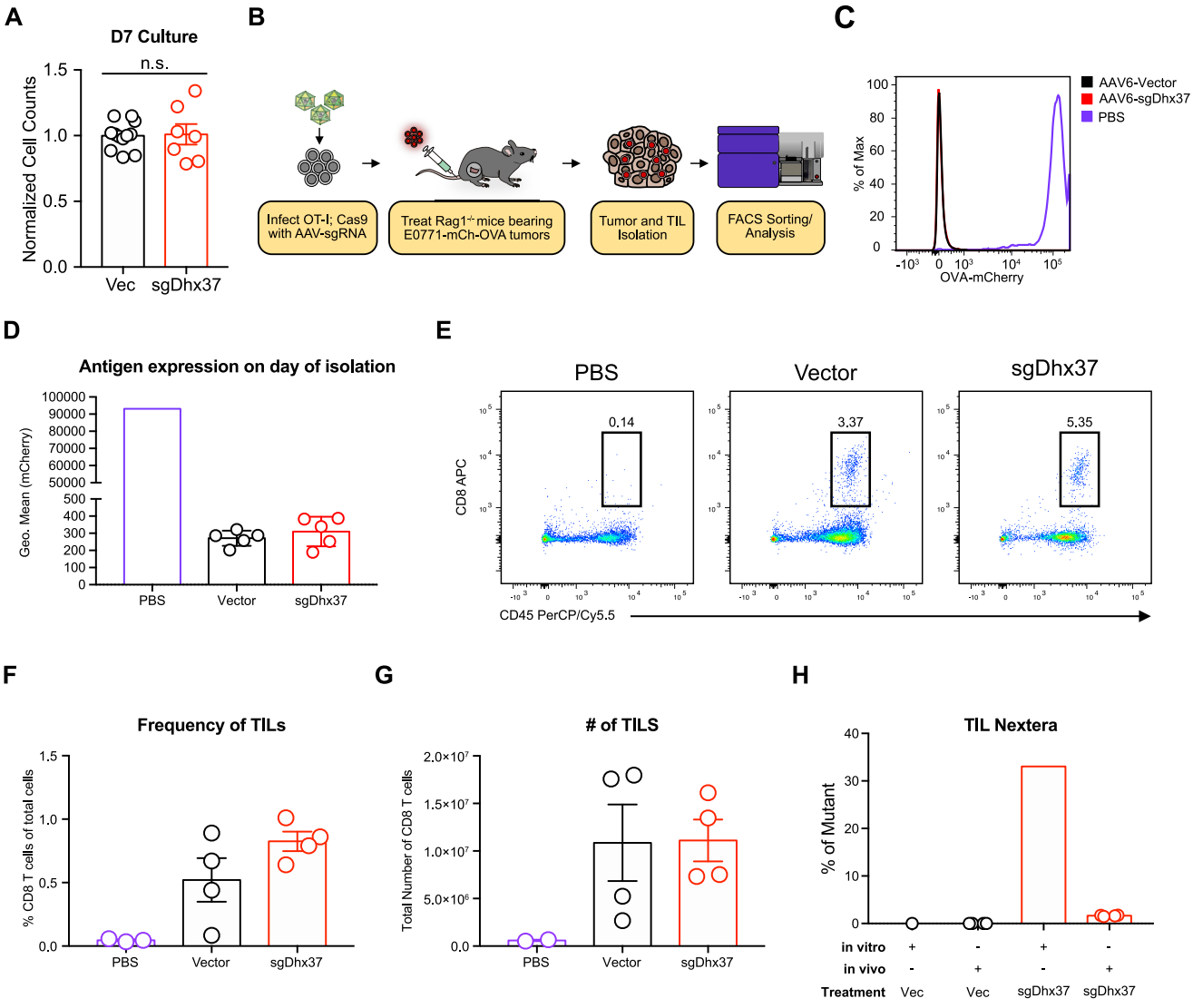


**Figure S4. Analysis of Antigen Retention and T Cell Stimulation Ability of Tumor Cells after Adoptive Transfer, Related to Figures 2 and 4**

(A) Normalized cell counts of AAV-Vector and AAV-sgDhx37 OT-I;Cas9 CD8 T cells after 7 days of cultures.

(B) Schematic of flow analysis experiment for antigen retention and T cell stimulation ability of tumor cells after adoptive T cell transfer.

(C and D) Flow cytometry plot of tumor cells gating on mCherry-OVA expression from tumors induced by E0771-mCh-OVA cancer cells treated with PBS, Vector or sgDhx37 OT-I;Cas9 CD8 T cells. (C) Representative histograms. (D) Bar plot quantification of (C).

(E) Flow cytometry plot of CD8 TIL gating for PBS, AAV-Vector, and AAV-sgDhx37 OT-I;Cas9 CD8 T cell-treated mice.

(F and G) Frequency and total numbers of CD8 TILs observed in *Rag1*$^{-/-}$ mice bearing E0771-mCh-OVA tumors treated with either PBS, AAV-Vector, and AAV-sgDhx37 OT-I;Cas9 CD8 T cells

(H) Representative Illumina targeted amplicon sequencing of the *Dhx37* sgRNA target site in AAV-treated OT-I;Cas9 CD8 T cells at the time of injection and on the day of tumor sample collection.

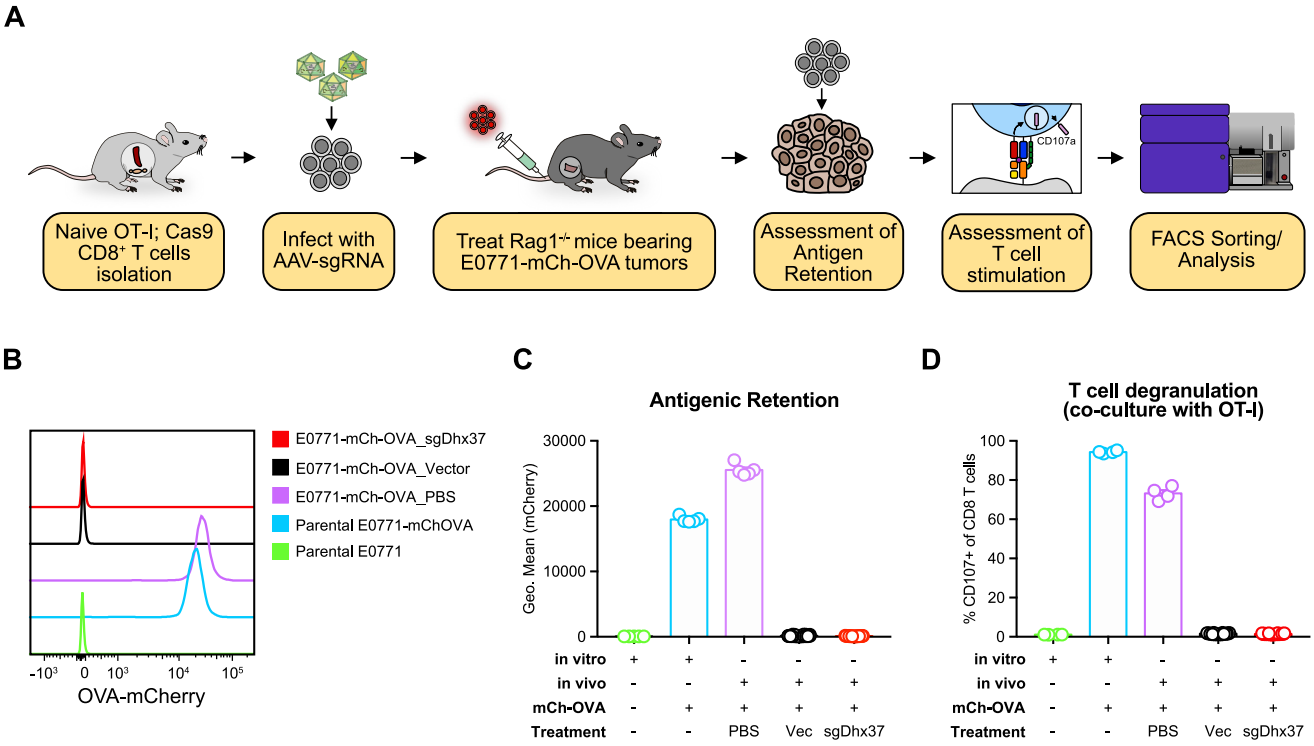


**Figure S5. Antigenic Retention and OT-I CD8 T Cell Stimulation by Tumor Cells *Ex Vivo*, Related to Figures 2 and 4**

(A) Schematic of flow analysis experiment for antigenic retention of cancer cells isolated from E0771-mCh-OVA tumor-bearing *Rag1*$^{-/-}$ mice treated with either PBS, AAV-Vector, or AAV-sgDhx37 OT-I;Cas9 CD8 T cells. Tumors were isolate 50 days after orthotopic tumor injection and cultured for several days in order to acquire sufficient number of cells for *in vitro* assays.

(B) Histogram representation of antigenic retention of cultured tumor cells on the day of experiment.

(C) Quantification of (B).

(D) Quantification of OT-I;Cas9 CD8 T cell degranulation when cocultured with indicated cancer cell.

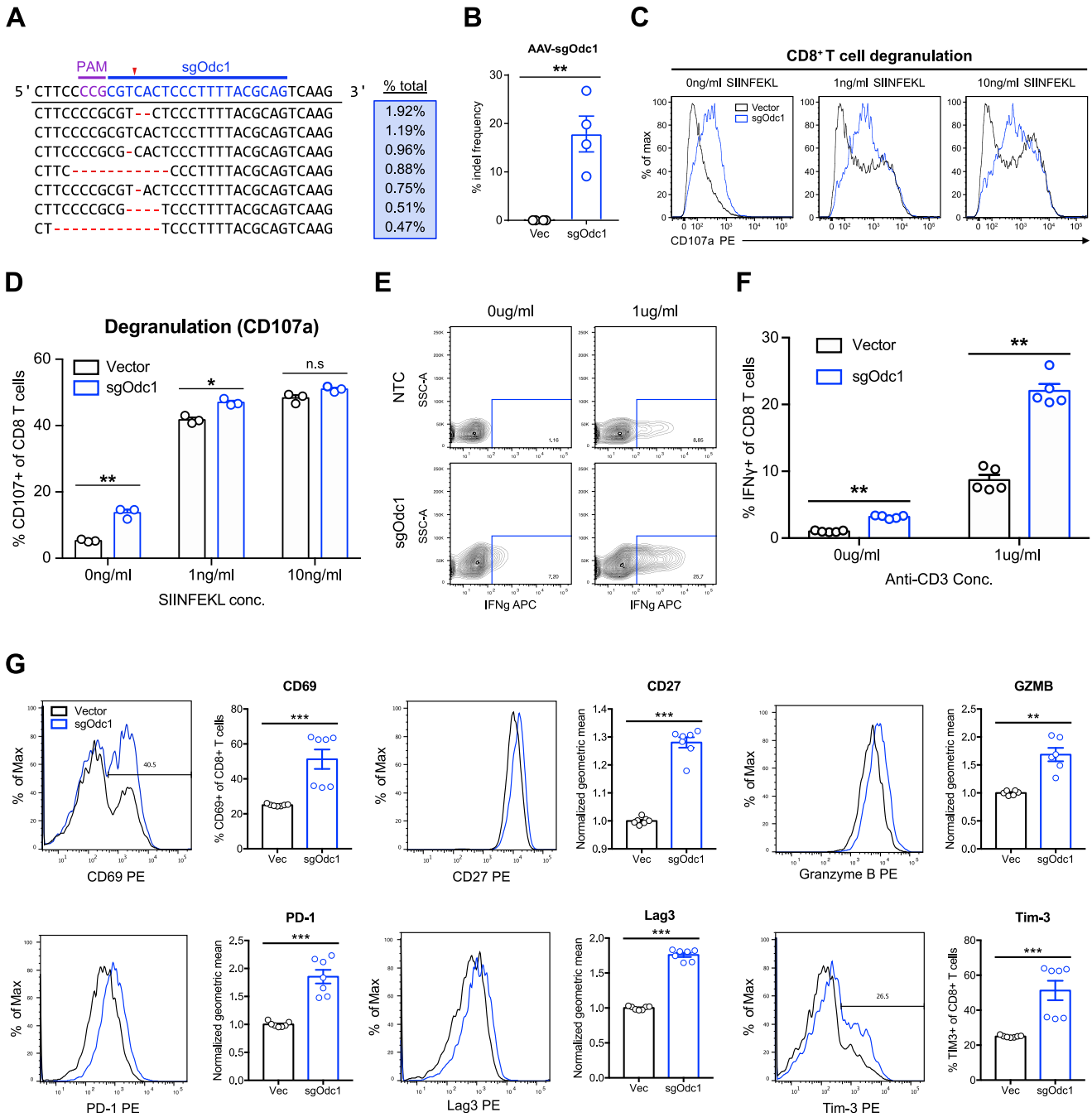


**Figure S6. Immunological Characterization of *Odc1* Knockout Mouse CD8 T Cells, Related to Figure 5**

(A) Representative Illumina targeted amplicon sequencing of the sgRNA target site 5 days after infection with AAV-sgRNA targeting the gene of interest. Top most frequent variants were shown, with the associated variant frequencies in the box to the right. In these Nextera-Indel plots, PAM and sgRNA spacers were indicated above. Red arrows indicate predicted cleavage sites. Red dash lines indicate deletions. Red A/C/G/T where applicable indicate insertions.

(B) Bona fide gene editing in primary murine CD8 T cells with an AAV-sgOdc1 measured by T7E1 surveyor assay. Data are shown as mean ± s.e.m.. ** = $p < 0.01$, by unpaired two-sided Mann Whitney test.

(C) CD107a degranulation assay for *Odc1* knockout CD8 T cells. Flow cytometry histograms were shown for each treatment group (Vector and sgOdc1) with 3 doses of SIINFEKL peptide pulsing of E0771 cancer cells (0, 1, and 10 ng/ml).

(D) Quantification of data from (C) with independent experimental replicates. Data are shown as mean ± s.e.m. ** = $p < 0.01$, by unpaired two-sided Mann Whitney test.

(E) Flow cytometry analysis plot of IFNγ production of sgOdc1 and Vector CD8 T cells with or without anti-CD3 stimulation.

*(legend continued on next page)*

(F) Quantification bar plot of (E). Data are shown as mean ± s.e.m.. ** = $p < 0.01$, by unpaired two-sided Mann Whitney test.
(G) Flow cytometry analysis of key immune markers of T cell function, including CD69, CD27, Granzyme B, PD-1, Lag3 and Tim-3. Left panel in each marker's analysis is a representative histogram of sgOdc1 (blue) and Vector (black) CD8 T cells. Right panel is a bar plot of quantification for each marker. Data are shown as mean ± s.e.m.. * = $p < 0.05$, ** = $p < 0.01$, *** = $p < 0.001$, by unpaired two-sided Mann Whitney test.

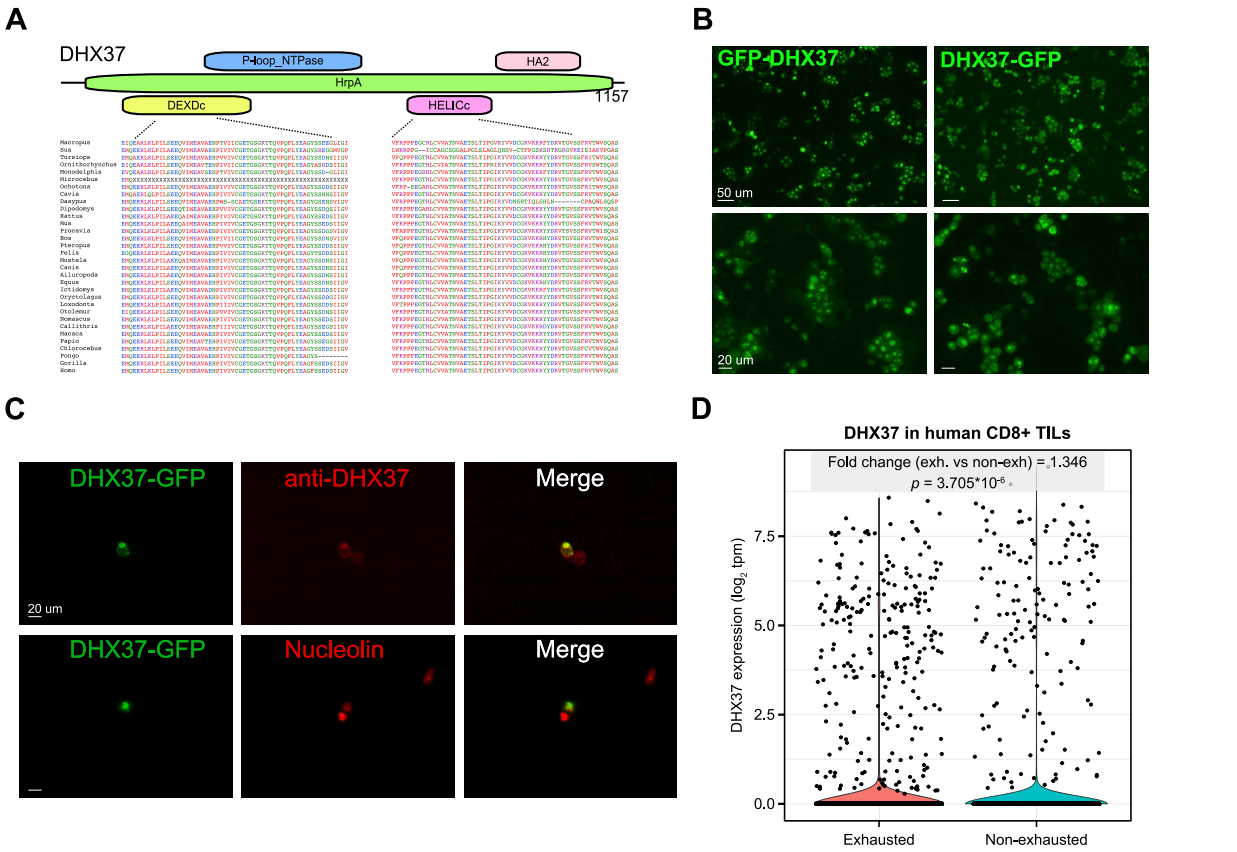


*(legend on next page)*

**Figure S7. Additional Analysis of Human DHX37, Related to Figure 7**

(A) Domain structure and conservation of DHX37 protein, which contains an HrpA domain that can be subdivided into 4 subdomains (DEXDc, P loop NTPase, HELICc and HA2). Shown below are representative alignments of regions in DEXDc and HELICc domains that are conserved between multiple mammalian species including mouse and human.

(B) Localization of DHX37 in the nucleus, as revealed by microscopic images of GFP-DHX37 and DHX37-GFP fusion proteins, under 20x (top) and 40x (bottom) objectives. Scale bars, 50 μm for 20x, and 20 μm for 40x.

(C) Co-Localization of DHX37 with nucleolus, as revealed by immunofluorescence of anti-DHX37, DHX37-GFP and Nucleolin staining, under 40x objectives. Scale bar, 20 μm.

(D) *DHX37* mRNA expression in human cancer patients' CD8 TILs. Exhausted TILs express higher level of *DHX37* ($p = 3.705e\text{-}16$ by Mann-Whitney test).

(E) Distribution of *DHX37* expression in human peripheral blood T cells, tissue-resident T cells, tumor-normal junction T cells, and tumor-infiltrating T cells in $CD3^+/CD4^+/CD25^-$ helper T cells, $CD3^+/CD8$ cytotoxic T cells, and $CD3^+/CD4^+/CD25^+$ regulatory T cells. The number and total percentage of $DHX37^+$ cells are noted on each plot.